NGU
Norges geologiske undersøkelse
Geological Survey of Norway

GEOLOGI FOR SAMFUNNET
GEOLOGY FOR SOCIETY

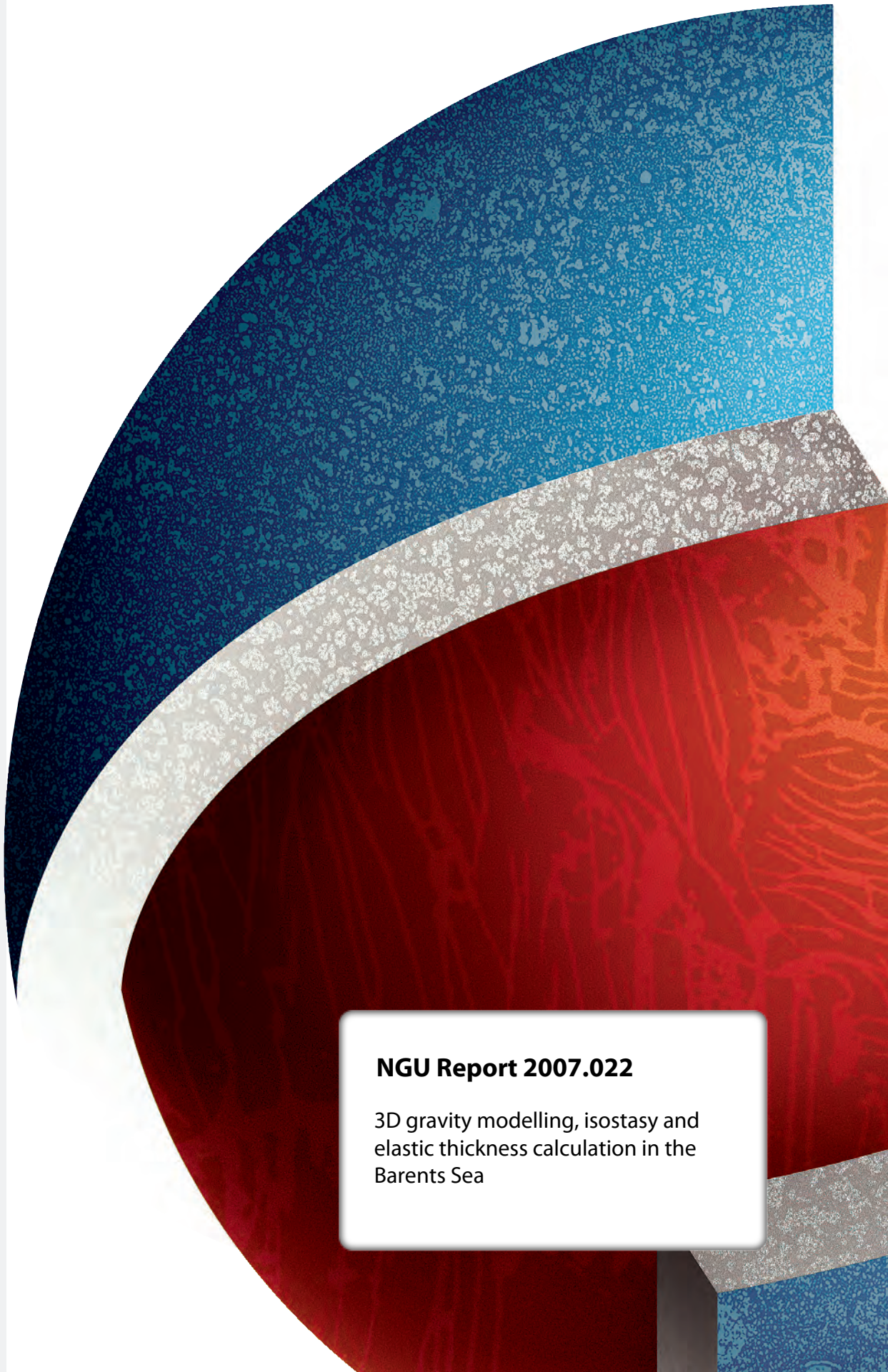

NGU Report 2007.022

3D gravity modelling, isostasy and elastic thickness calculation in the Barents Sea

REPORT

Geological Survey of Norway
N-7491 Trondheim, Norway
Tel.: 47 73 90 40 11
Telefax 47 73 92 16 20

Report no.: 2007.022 | ISSN | Grading: Confidential until 31.12.2009

Title:
3D gravity modelling, isostasy and elastic thickness calculation in the Barents Sea

Authors:
Susann Wienecke, Jörg Ebbing & Laurent Gernigon

Clients:
StatoilHydro, NFR

County:

Commune:

Map-sheet name

Number of pages: 56 Price (NOK):
Map enclosures:

Fieldwork carried out:

Date of report:
01.06.2007

Project no.:
3133.00/3127.00

Person responsible:

Summary:

Integrated 3D density and isostatic modelling show that a large difference exists between the Eastern and Western Barents Sea in terms of physical properties in the crust and underlaying mantle. To constrain our analysis we make use of a 3D density model based on the velocity model BARENTS50. The density model provides information about the crustal configuration, e.g. the Moho and the loading of the crust including all internal density variation. The calculated gravity anomalies (computed from these density variations) cannot be adjusted to the observed gravity field. Therefore the effect of the Earth's curvature on the gravity calculation was investigated by a coordinate transformation and projection of the 3D model into a spherical 3D model. The error between the modeled and the observed gravity remains significantly large. The missing masses, which are needed to minimize the difference, are supposed to be located not only in the crust but also in the mantle. High-density material (>3300kg/m^3) is needed below the Eastern Barents Sea in order to isostatically balance the masses from the thick crust and also to fit the observed gravity field. The isostatically calculated mantle densities correlate well with other results and confirm the lage difference between the Eastern and Western Barents Sea.

In a next step we apply the analytical solution for an elastic plate (ASEP), which solves the 4^{th} order differential equation for the flexure of a thin plate to the Barents Sea. The ASEP allows us to calculate the flexure Mohos, and by comparison with the reference Moho, the elastic thickness distribution. The results are used to validate tectonic concepts, e.g. the location of the proposed Caledonian suture. The elastic thickness distribution indicates a weak crust in the Western Barents Sea, which correlates with the idea of rifted basins, while the Eastern Barents Sea is characterized by a rigid crust typifying a stable continental platform.

In the past the elastic thickness has been used synonymously for the flexural rigidity, since it was defined by the material parameters of Young's modulus and Poisson ratio, which were assumed to be constant. However, concerning the vertical and horizontal variation of crustal composition, which corresponds to a change of Young modulus by orders of magnitude - the use of a constant standard value in the calculation process is doubtful. For that reason the elastic thickness distribution was recalculated including the Young's modulus variation, estimated by using the p-wave velocities of the Barents50 model. The results show a better correlation with the geological and tectonic features.

Keywords:		
Geophysics	Continental shelf	Gravimetry
Basement	Flexural rigidity	Moho

1 INTRODUCTION

The present report documents the results related to a 1 ½ year PostDoc work from S. Wienecke in the projects "Basement Characterization Barents Sea and Svalbard" and "BASIC: Barents Sea and Intra-Cratonic basins" financed by the Geological Survey of Norway, the Norwegian Research Council and Statoil. The work is related to the study of the isostatic state of the Barents Sea region by interpretation of the gravity field observation in terms of density modelling and calculation of elastic thickness distribution.

For the last decades, research and petroleum exploration in the Barents Sea have revealed a complex sedimentary and crustal architecture influenced by a variety of long-lived tectonic processes. Nevertheless, a large part of the BarentsSea region remains underexplored. Furthermore, crustal architecture and tectonic evolution in the Barents Sea are still poorly constrained and the supposed ideas about the geological history are controversial (e.g. Breivik et al., 2005; Faleide et al., 1988; Fichler et al., 1997; Gee, 2005; Gudlaugsson et al., 1987; Johansen et al., 1992; Torsvik and Andersen, 2002).

The Barents Sea has been tectonically influenced by major continental collision and a complex rift history leading subsequently to continental breakup in Cenozoic time (Gudlaugsson et al., 1998). The main collision event, in Caledonian time culminated approximately 400Ma (Gee, 2005). This collision resulted in the consolidation of the Laurentian plate and the Baltic plate into the Laurasian continent and the closure of the Iapetus Ocean (Pickering and Smith, 1998). The eastern side of the Caledonides is flanked by the Timanides, a Late Neoproterozoic foldbelt, recognized, from the Finmark Platform up to the Timan-Pechora and Novaya-Zemlya region.

The Eastern Barents Sea was subsequently affected by a younger collision phase between the Laurentsian continent and Western Siberia that culminated latest Permian-earliest Triassic. The Ural orogen mostly affects the eastern part of the Barents Sea. The Ural mountain chain and its proposed northern extension, Novaya Zemlya, define the suture zone of this thrustbelt (Gee and Pearse, 2006). The Late Paleozoic and Mesozoic tectonic history of the Barents Sea was mostly dominated by extensional tectonic, which was initiate with the end and post-orogenic gravity collapse of the newly formed Caledonian and Uralian orogenic belts (Crowley et al., 2000; Gee, 2005). Several rift episodes have

been documented in the Early-Middle Devonian, Carboniferous, Permian, Triassic and late Jurassic-Early Cretaceous (Johansen et al., 1992).

Timanian, Caledonian an Uralian trends dominate the basement architecture and influenced the rift and basin configuration of the Barents Sea (Fichler et al., 1997). Caledonian influences are seen in the N-S structural grain of the western Barents margin and Svalbard, furthermore the NE-SW grain of the southwestern Barents Sea and Finnmark. The most significan sedimentary basins, in terms of thickness and lateral extent lie in the russion sector. The foreland basins immediately west of Novaya Zemlya were formed in the foredeep zone to the Uralian thrustbelt. The western margin of the Barents Shelf bordering the continent-ocean transition is characterized by a shear margin developed between north Greenland and the western margin of the Barents Shelf. Large thicknesses of Cenozoic sediments were deposited in this area (Johansen et al., 1992). Summarizing, the study area in the Barents Sea is characterized in the western part by the ocean-continent transition, the Svalbard transition and relatively small sedimentary basins compared to the eastern part, which contains large-scale sedimentary basins like the Northeast and Southeast Barents Basin and the foreland basins of Novaya Zemlya (Figure 1).

Since the Barents Sea has been affected by a long and complex tectonic history, should this left its signature within the crust and lithosphere. Potential field data and integrated 3D density modelling, isostatic considerations and as well their interpretation in terms of flexural rigidity/elastic thickness calculation allow us to identify regions with different petrophysical properties, which may reflect sutures, deformation and rift zones. Particularly, the location and directions of faults and tectonical units can correlate well with areas where a rapid change of elastic thickness values is obtained (Wienecke, 2006; Wienecke et al., 2007).

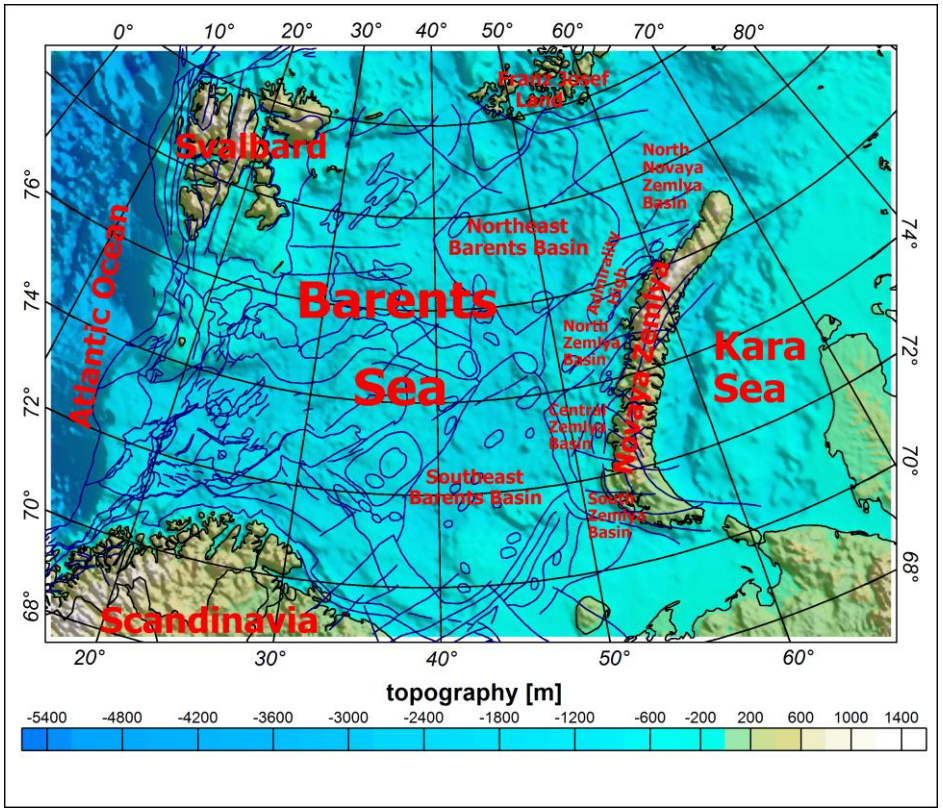

Figure 1 *Topography and main structures in the Barents Sea.*

The present report documents the gravity and isostatic modeling and as well the development of the necessary formulas. The theoretical, physical background is adressed and preliminary interpretations of the results are given.

This report aims not to accomplish a deep interpretation of the results in terms of geological/tectonic history.

1.1 Input Data

1.1.1 Gravity

We make use of the Arctic Gravity Project data compilation that consists of free-air anomalies offshore and Bouguer anomalies onshore (International Association of Geodesy, 2002). The Bouguer gravity for the entire working area (see Fig. 2) was calculated with a reduction density of 2670 kg/m and additionally the ice cover on Novaya Zemlya was taken into account (Ebbing et al., 2007). The Arctic Gravity Project provides gravity data derived from airborne, surface and submarine data in the Arctic from a multitude of sources (http://earth-info.nga.mil/GandG/wgs84/agp/).

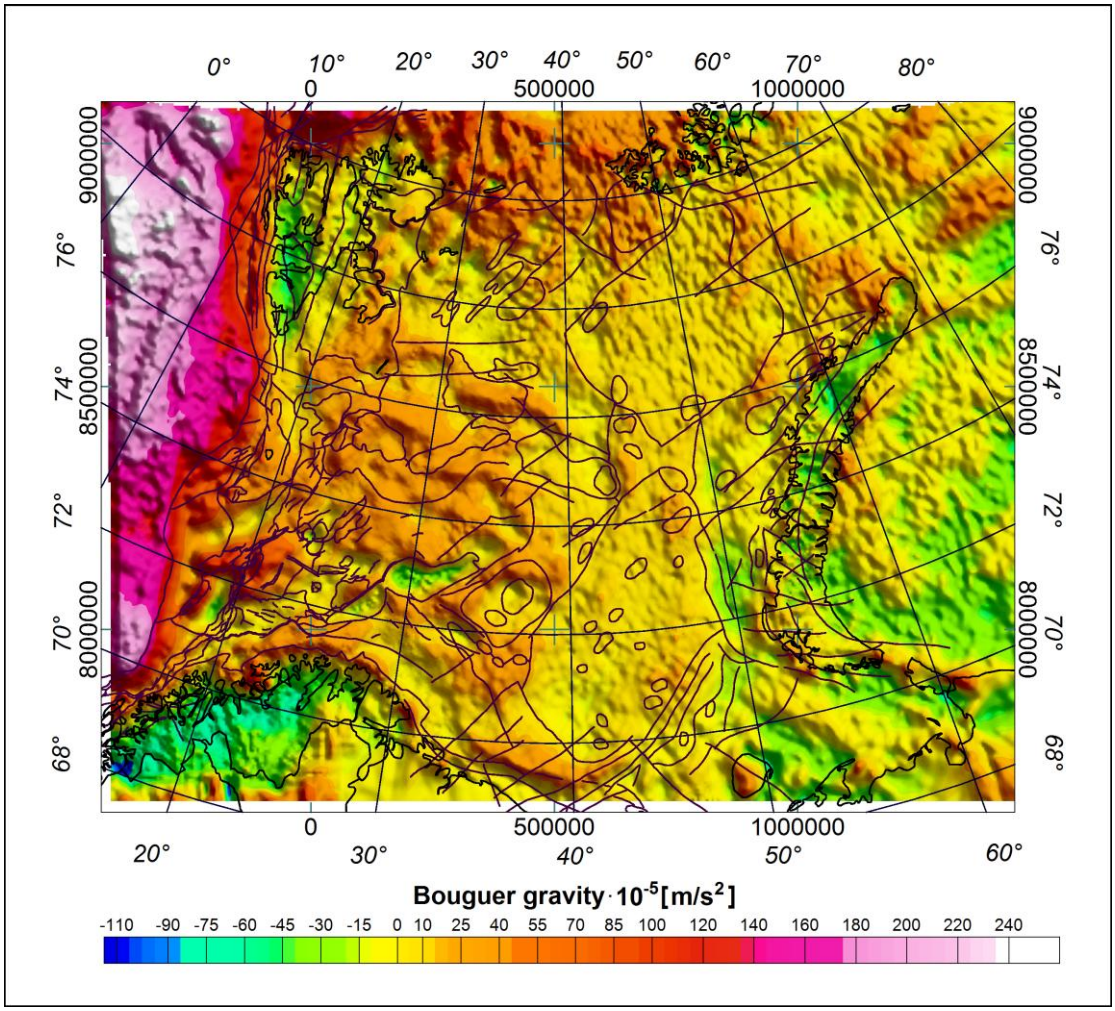

Figure 2 *Bouguer gravity anomaly, calculated from Arctic Gravity Project with 10 km spatial resolution.*

1.1.2 Velocity Model

The seismic velocity model is a compilation from the University of Oslo and NORSAR (Faleide et al., 2006) from all available seismic and seismological observations. The model is called BARENTS50 model and is defined in columns with a spatial resolution of 50 km. It is constrained by 2D wide-angle reflection and refraction lines and additional passive seismological stations. The final compilation has a precision of 8.4% error for coordinates, 7.5% error for the heights, depth and thickness and an error of 10.4% for the velocity and density-values (Ritzmann et al., 2006).

2 GRAVITY MODELING

2.1 Start model

The velocity model BARENTS50 was read out with a self-made Fortran routine. The output are surfaces , the coordinates are transformed and projected with datum ED50 Finland/Norway, Ellipsoid International 1924, to 37N Universal Transverse Mercator zone. These surfaces are used as layers in a 3D density model. The gravity forward modeling is done with the software GMSYS3D from Geosoft. In view of the fact, that the Bouguer gravity is modeled, the water density was replaced by the reduction density 2670 kg/m^3. The model consists of 7 layers. In a first step a constant density between each layer was used (see Table 1).

layer	**density in kg/m^3**	**comments**
water	1030	Replaced with 2670 kg/m^3
upper sediments	2200	corresponds to bathymetry
lower sediments	2500	
upper crystalline crust	2700	
middle crystalline crust	2850	
lower crystalline crust	3200	
Moho	3280	
sampled mantle model	-	not taken into account

Table 1 *Presentation of layers and parameters, which are used in the 3D model*

The first layer represents the water surface. The second layer represents the topography and bathymetry. Instead of using the information from the BARENTS50 model the topography/bathymetry grid based on the ETOPO data set available at NOAA/USGS is used, since it has a better spatial resolution (Figure 3).

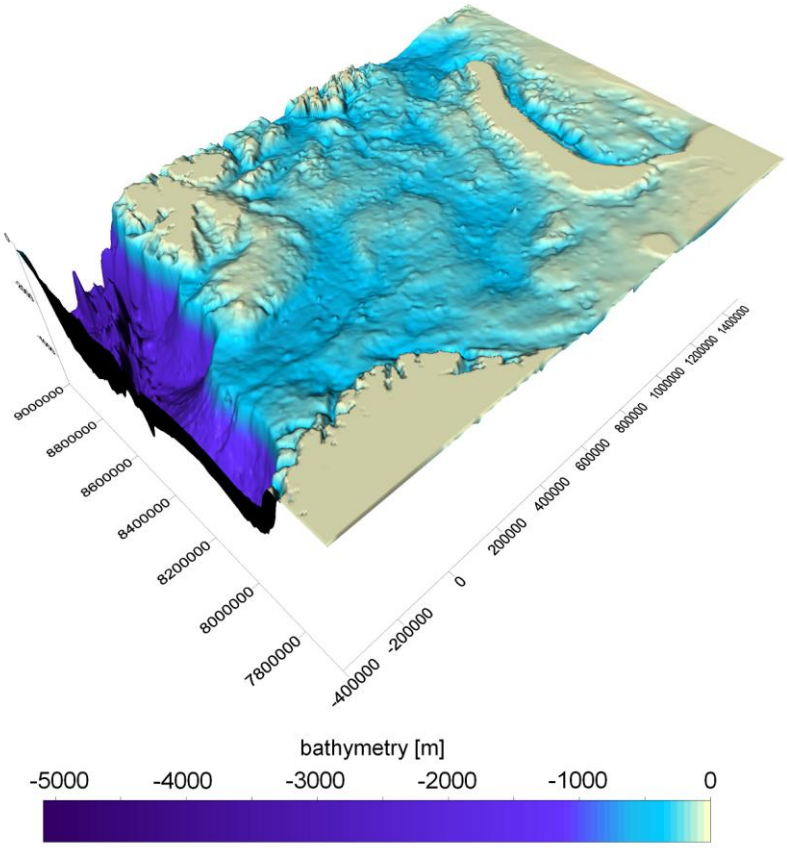

Figure 3 *Second layer of the density model corresponding to topography/ bathymetry.*

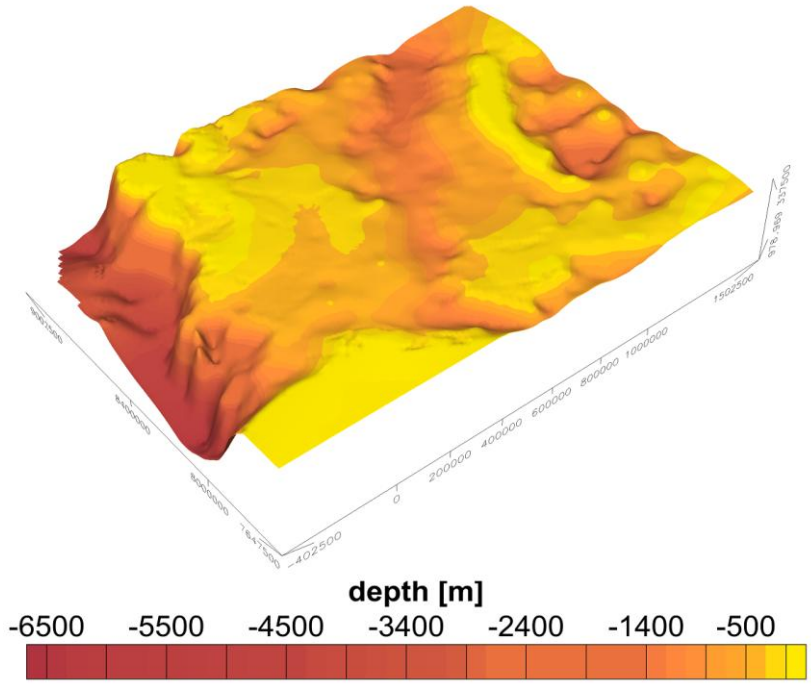

Figure 4 *Third layer of the density model corresponding to the boundary between upper and lower sediments.*

The third layer represents the boundary between upper and lower sediments (Figure 4). The depth to the top of the lower sediments ranges from –6500 m till –100 m. The sediments deepen approximately –3000 m in the middle part of the study area westwards from Novaya Zemlya and eastward from it. The deepest values are reached at the western margin of the study area. The depth values change rapidly at the ocean-continent boundary.

The lower crust is divided in 3 layers: upper basement, middle basement and lower basement. The fourth and fifth layer (Figure 5, Figure 6) representing the upper and middle basement are characterized by a halfmoon-shaped depression below the Eastern Barents Sea basins (westward Novaya Zemlya). The upper basement shows an upwelling at Novaya Zemlya, Finnmark and parts of Svalbard. The depth to the middle basement decreases in the area of the ocean-continent transition to the west. The sixth layer representing the lower basement (Figure 7) is relatively flat and shows a different geometry compared with the upper and middle basement. The upwelling at the western margin is related to the ocean-continent transition. The prominent halfmoon-shaped feature that correlates with the location of the Eastern Barents Sea basins disappears.

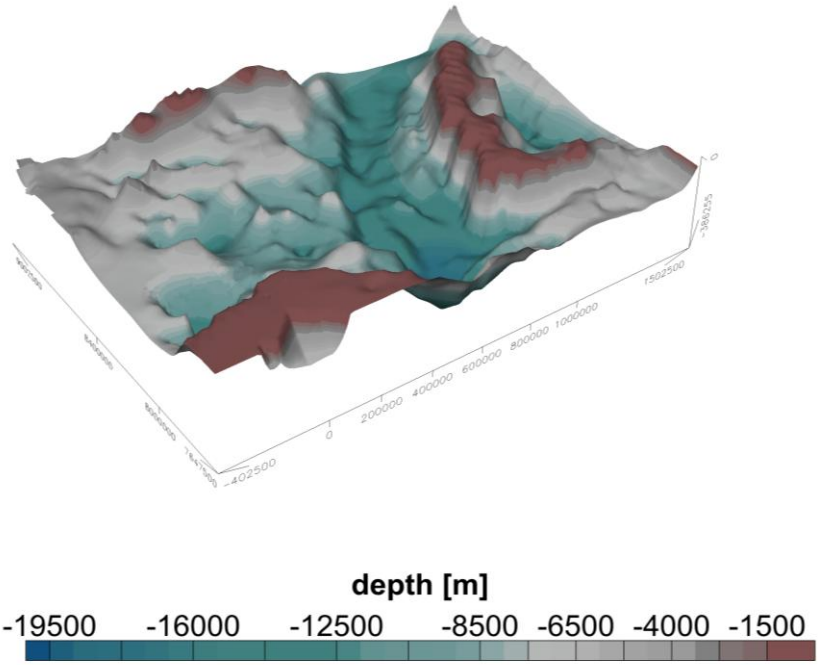

Figure 5 *Fourth layer of the density model corresponding to the top of upper basement.*

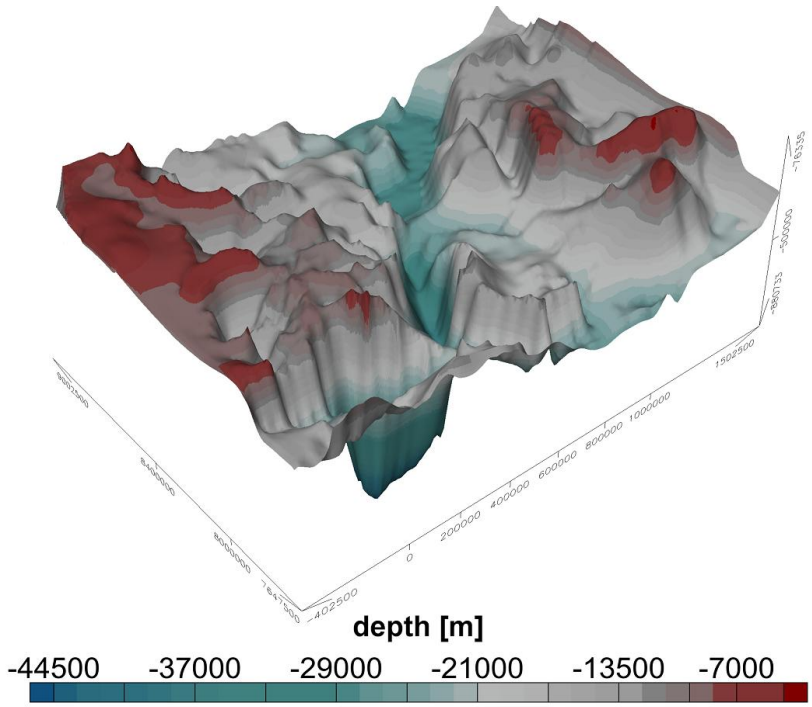

Figure 6 *Fifth layer of the density model corresponding to the boundary between upper and middle basement.*

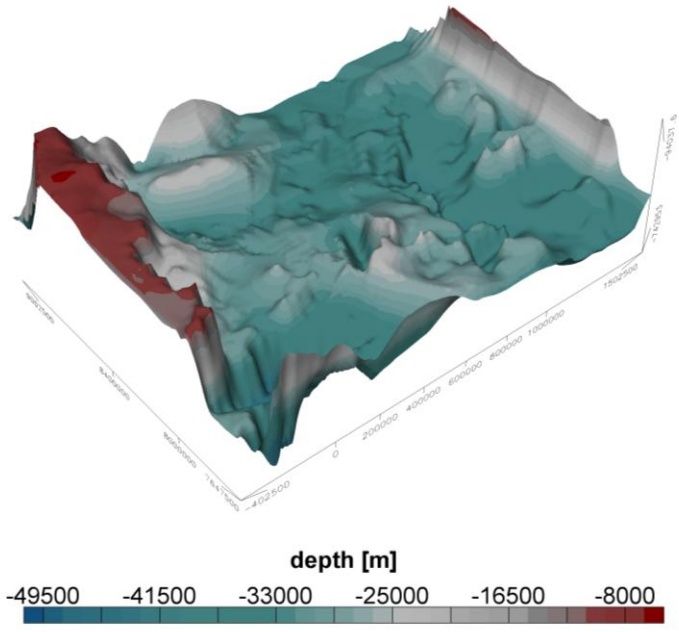

Figure 7 *Sixth layer of the density model corresponding to the boundary between middle and lower basement.*

The seventh layer, which represents the Moho discontinuity is characterized by relatively small undulations in depth values (<5km) from the Atlantic continent-ocean-boundary in the west to Novaya Zemlya in the east (Figure 8). Obviously the Moho geometry does not

correlate with the basement geometry. The Moho depth values in the Western Barents Sea (32.5-35 km) are exiguous less than in the Eastern Barents Sea (35-37.5 km).

The main changes are related to the onshore-offshore transition in the south were the Moho depth values rapidly becomes larger than 40 km. The Moho beneath Novaya Zemlya reaches depth values of 45 km in the central and up to 50 km in the western part. At the western edge the Moho depths decrease to 10 km because of the continent-ocean transition. This Moho is used as reference Moho for the rigidity estimates (see Chapter 3).

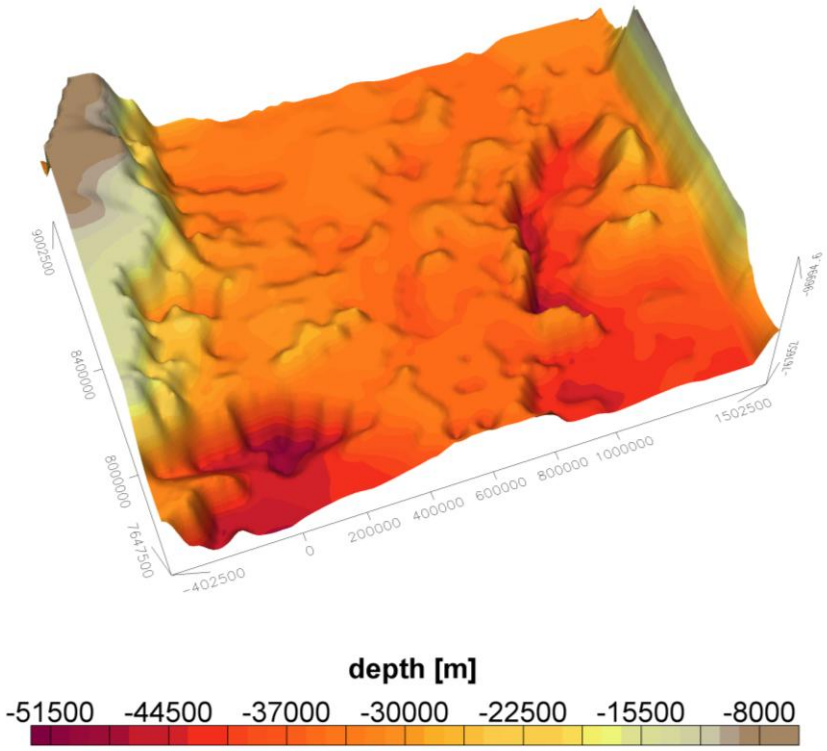

Figure 8 *Seventh layer of the density model that represents the Moho.*

2.2 Gravity effect of 3D model with constant density

The seven layers (Figure 3 - Figure 8) are the input grids for the 3D density model in order to calculate the gravity effect with the GMSYS-3D software (Popowski et al., 2006). For each layer a constant density was used (see ***Table 1***).

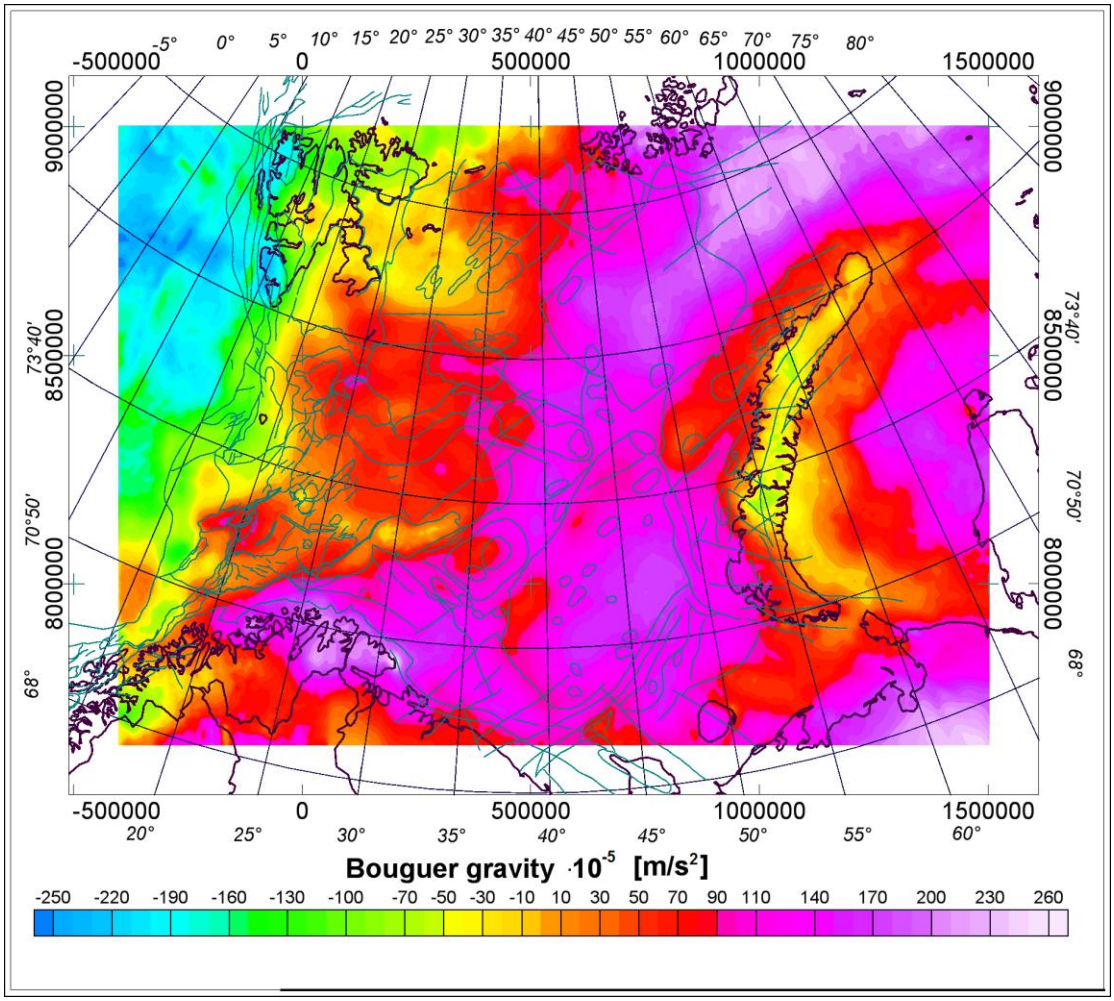

Figure 9 *Error between the observed and calculated gravity effect for the density model with constant density for each layer*

The error between the calculated and observed gravity effect is around 200 $\cdot 10^{-5}$ m/s^2 in the Eastern Barents Sea, 30 till 100 $\cdot 10^{-5}$ m/s^2 in the western Barents Sea and -130 to -200 $\cdot 10^{-5}$ m/s^2 in the area of the ocean-continent transition. To achieve a better fit between the calculated and the observed gravity either the geometry or density of the model has to be changed. Consequently the information from the velocity model about the density variation will be included in the next step. The original data from the BARENTS50 model has data gaps (see Figure 10 till Figure 12). The missing data points were filled by interpolation using the Kriging method.

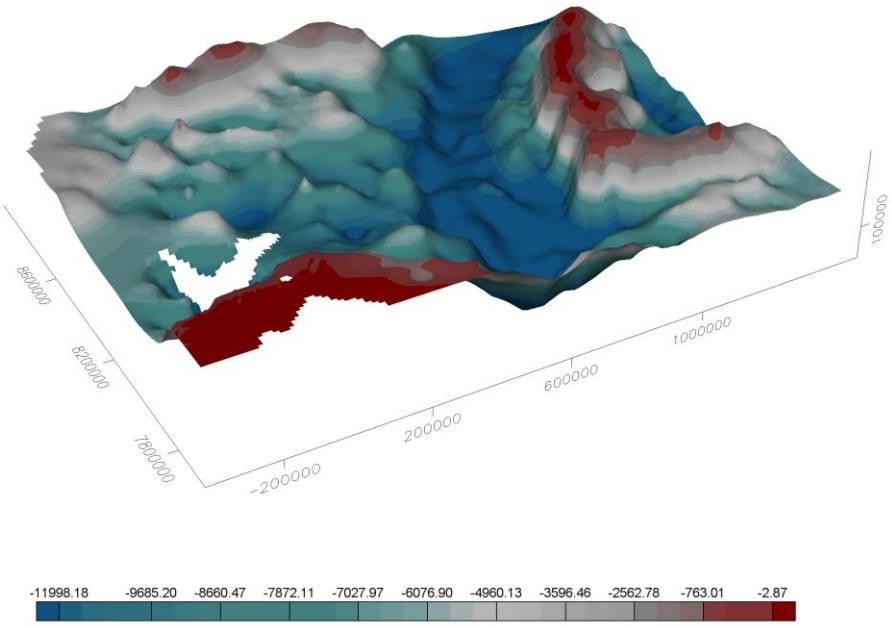

Figure 10 *In the upper basement information is missing about the depth in the southwestern part of the study area.*

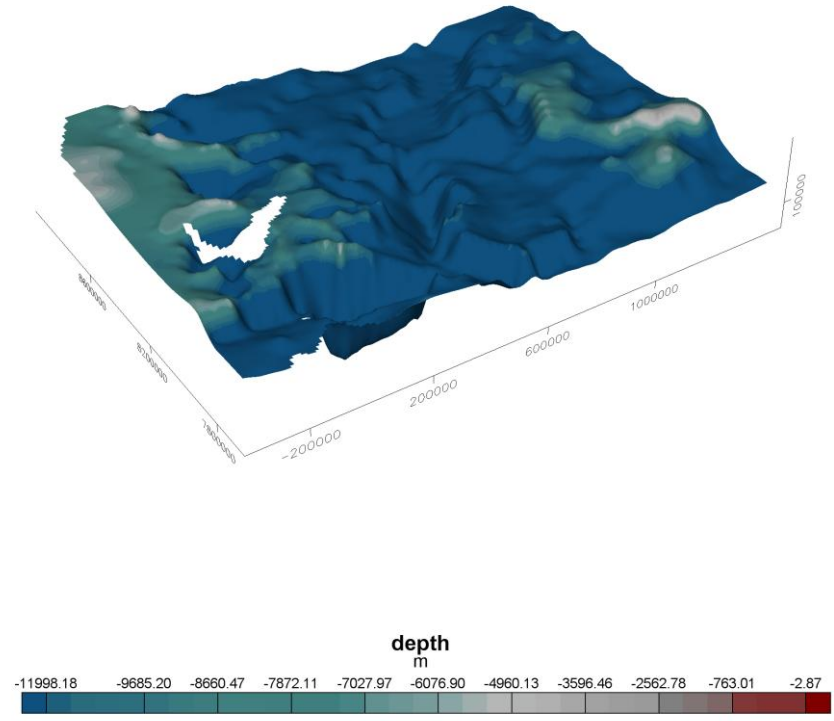

Figure 11 *In the middle basement information is missing about the depth in the southwestern part of the study area.*

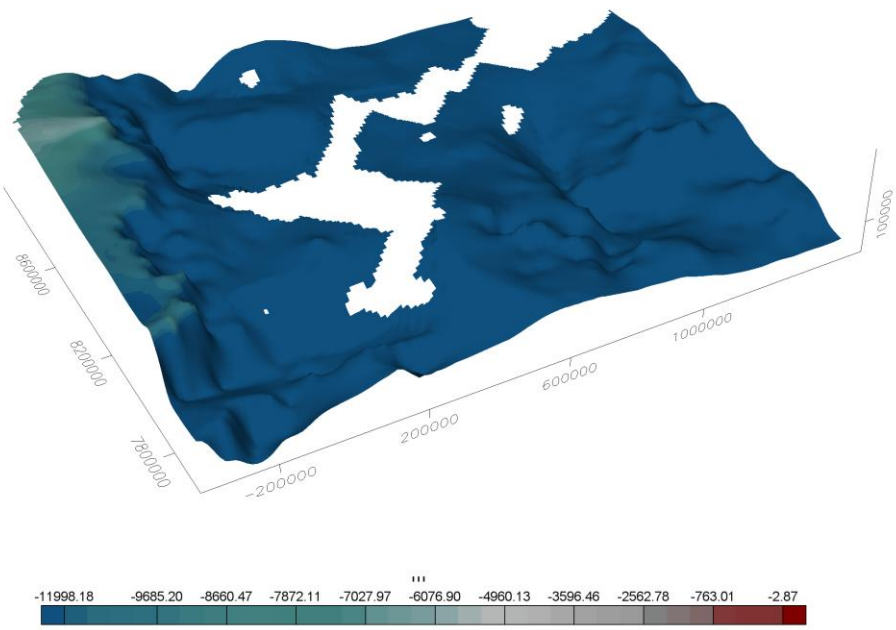

Figure 12 *In the lower basement a large amount of information is missing about the depth in the middle part of the study area.*

2.2.1 Comparison of depth to basement estimates

Available top basement maps or data for the Barents Sea are mainly based on aeromagnetic depth source estimates (Skilbrei, 1991; Skilbrei, 1993) and a combination of these with shallow and deep seismic lines (Gramberg et al., 2001; Johansen et al., 1992). These compilations cover either the Western or the Eastern Barents Sea, but only to a limited extent the transition zone between the two areas.

The top to basement map by Skilbrei has a high resolution (5x5km), but covers only the south-western Barents Sea (Skilbrei, 1993). The top to basement map of the Barents50 model has a lateral resolution of 50 km (Ritzmann et al. 2007). Accordingly the top to basement map by Skilbrei (1993) was interpolated to a lower resolution of 50 km. Comparison of these two maps shows a difference in depth values ranging from -9 to 5 km for the Western Barents Sea (Figure 13).

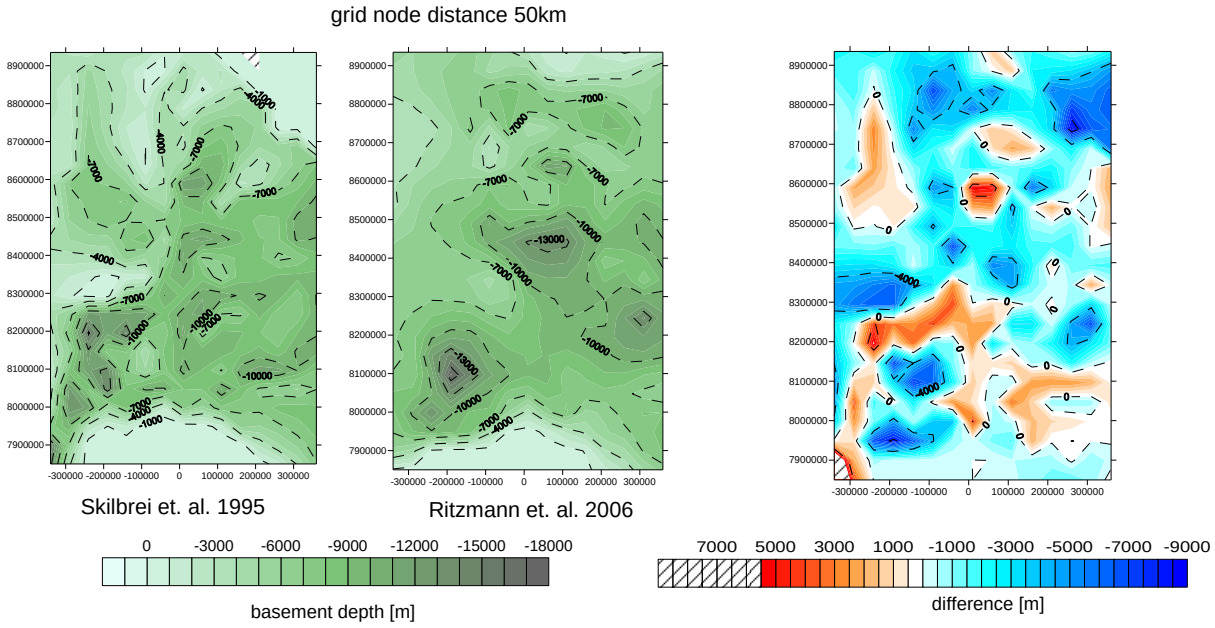

Figure 13 *Comparison of top to basement maps in the Western Barents Sea.*

Comparison of top basement maps in the Eastern Barents Sea compiled by Gramberg *et al.* (2001) with the BARENTS50 model shows a difference in depth values ranging from -18 km to 8 km.

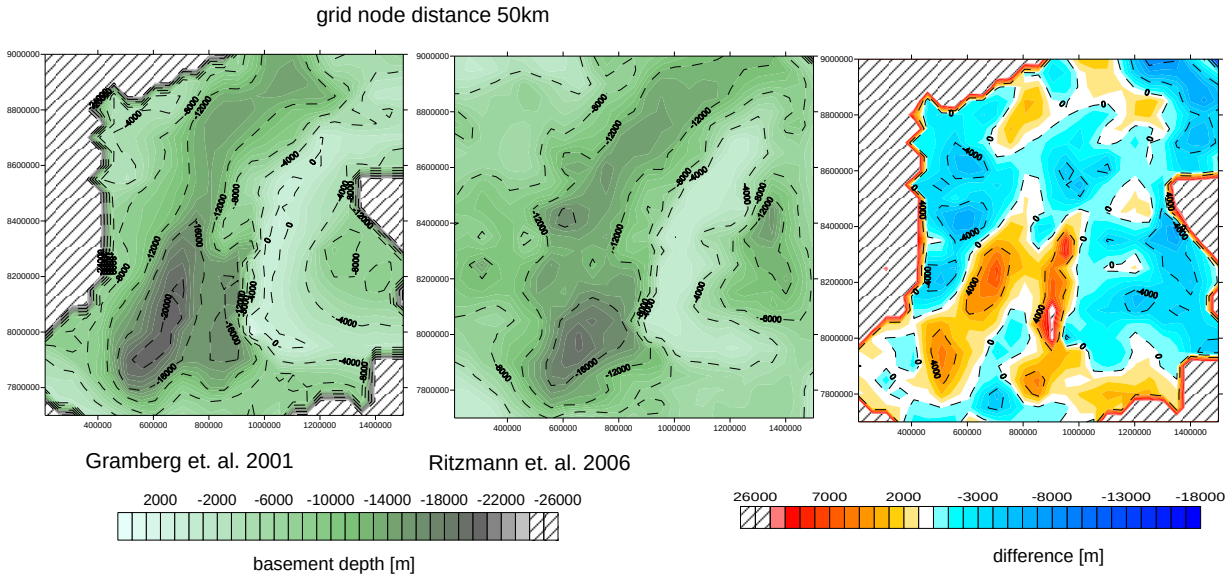

Figure 14 *Comparison of top to basement maps in the Eastern Barents Sea*

In order to provide a better density model the geometry of the basement should be further investigated and constrained along available seismic lines. This is a task for future work.

2.3 Gravity effect for density variation within the crust

The horizontal density variations from the velocity model BARENTS50 were transferred into grids readable with e.g. Geosoft and Surfer, which contain information of the lateral density variation. These grids are now the input for the GMSYS-3D software in order to calculate the gravity effect of the 3D density model.

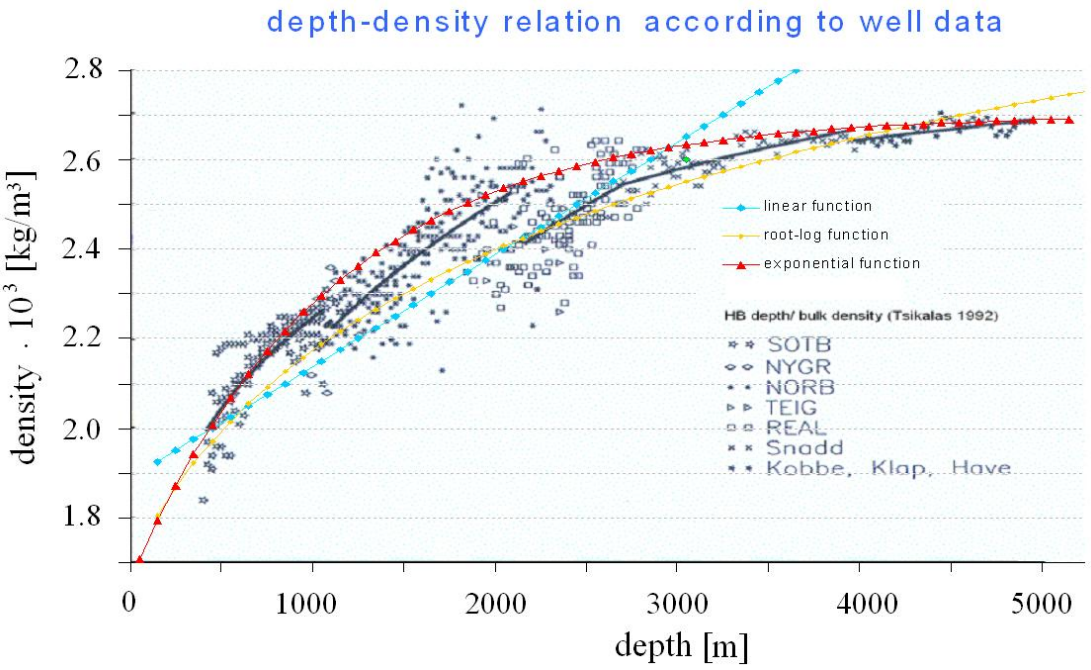

Figure 15 *Exponential depth-density function (red colored) constraint by well data.*

For the densities of the sediments we use instead of a linear relationship a modified density-depth function after a sediment compaction model (Braitenberg et al., 2006; Wienecke et al., 2006), by assuming an equal depth decay parameter ($b=b_1=b_2$):

$$\rho(d) = \Phi_0 \cdot e^{-b_1 d} \rho_f + (1 - \Phi_0 \cdot e^{-b_2 d}) \rho_g \qquad \text{(Eq. 1)}$$

with ρ as density, d as depth d and Φ as porosity. The relevant parameters of fluid density $\rho_f = 1030\,\text{kg/m}^3$ grain density $\rho_g = 2700$ kg/m^3, starting porosity Φ_0=0.6 (which corresponds to 60% porosity at the sediment surface) and the depth decay parameter b = -0.9 of the exponential density-depth relation are chosen in order to adjust the exponential function to the density values according to borehole information in the Western Barents

Sea (Tsikalas, 1992).

Figure 15 shows the exponential depth-density relation applied to the sediments. The common used linear relationship cannot be used to describe the sediments (see Fig 6), because at a depth of e.g. 4000 m the density value would increase to more than 2900 kg/m^3. This is a higher density value then the subjacent basement underneath and accordingly would the implementation of a linear function produce a pseudo-anomaly at greater depth.

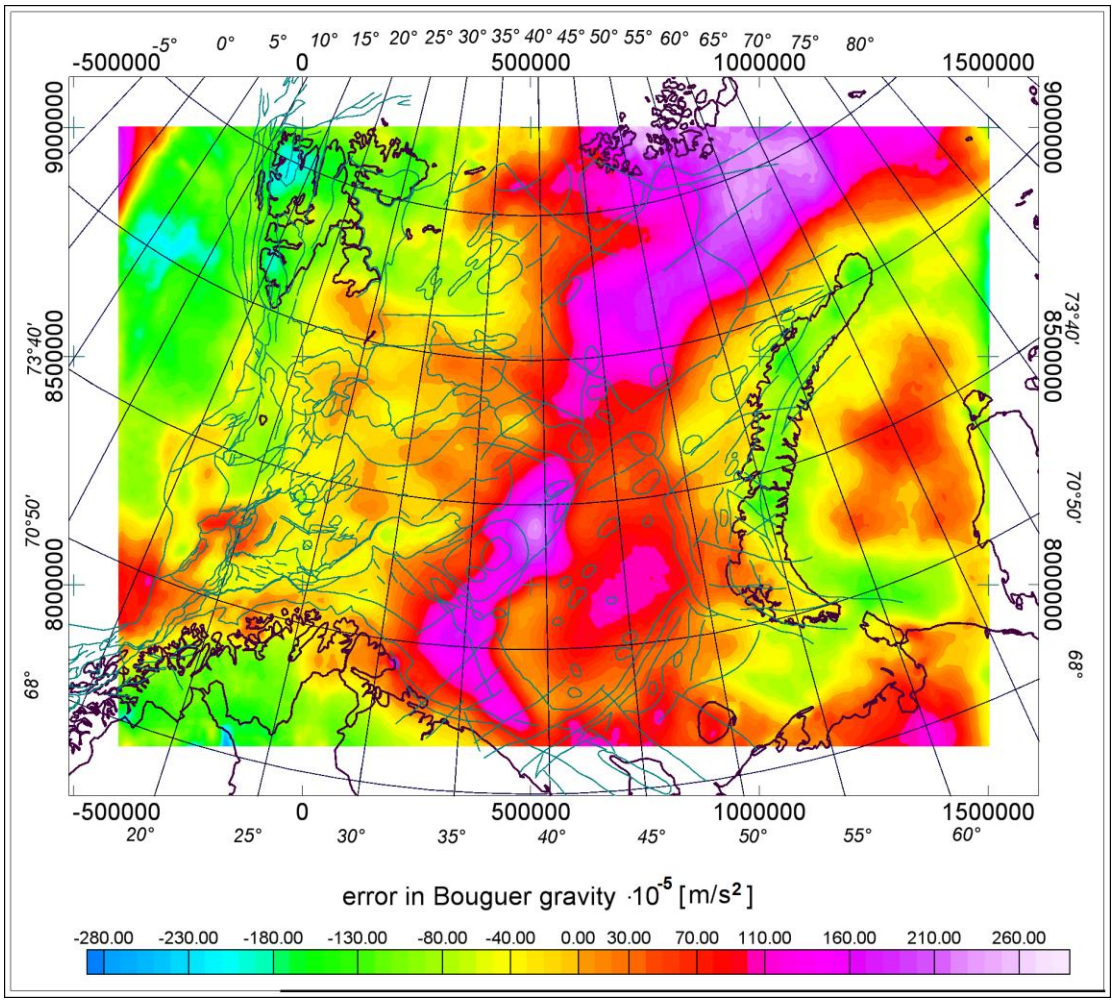

Figure 16 *Error of the calculated Bouguer gravity with variable densities and the observed Bouguer gravity in the Barents Sea region.*

The calculated gravity effect of the 3D model fits the regional gravity observations better than the previous 3D model with constant density (Figure 16). Nevertheless, the error between the modelled and the observed gravity is still significantly large. The discrepancy in the level of modelled and observed anomalies is approximatly -130 mGal in the Western

Barents Sea, and 160 mGal in the Eastern Barents Sea. However, a wide range of values for the density variation in the upper crustal structure was used, which is constrained by the velocity model BARENTS50.

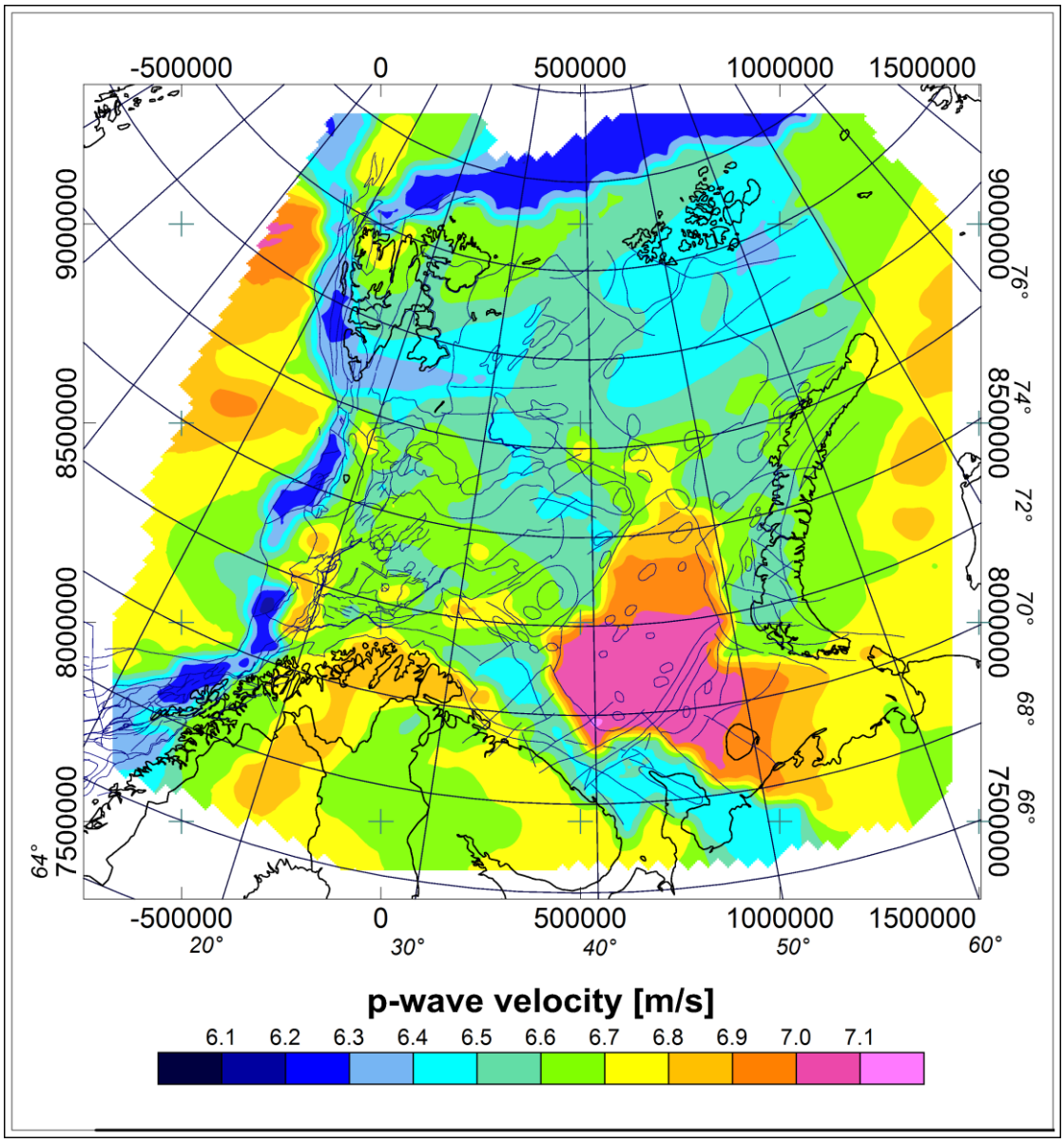

Figure 17 *Distribution of P-wave velocities in the middle basement (middle crust).*

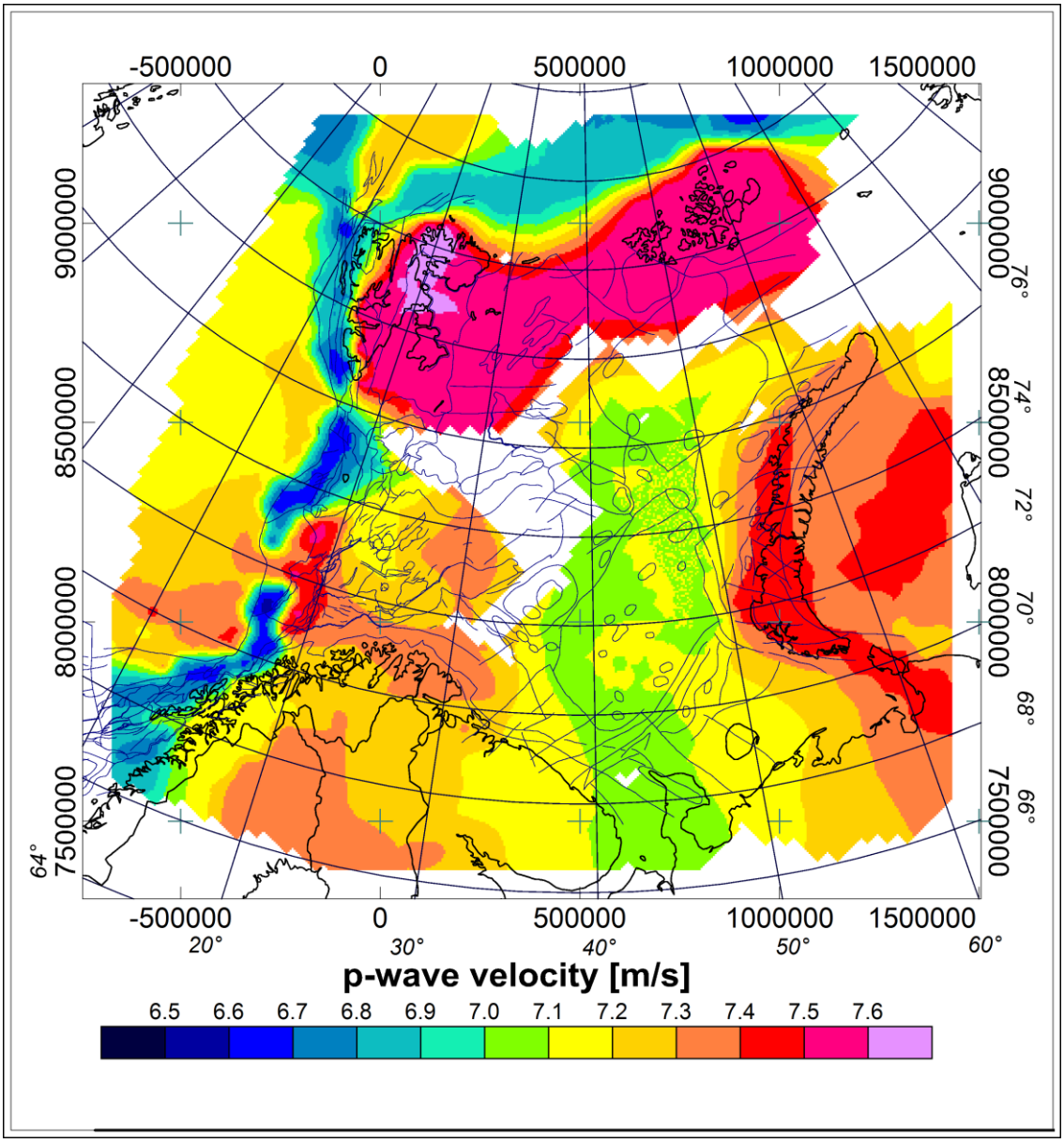

Figure 18 *Distribution of P-wave velocities in the lower basement (lower crust).*

The middle and lower basement, for example, show a wide variation of the p-wave velocities from 6.28-6.98 m/s in the middle basement and 6.72-7.56 m/s in the lower basement (Figure 17 and Figure 18).

In the area of the Eastern Barents Sea a body with higher velocities is obtained in the middle crust. This body disappears in the lower crust. This could be an interpolation artefact of the BARENTS50 model, since several layers had to be combined by taking the average of the velocities (pers. comm. Ritzmann).

For this reason, the missing masses, which are needed to adjust the level difference- are supposed to be located not only in the crust but also in the mantle. To distinguish between the two possibilities we study the isostatic state of the model and try to balance our model

on a lithospheric scale (Ebbing et al., 2007). Another effect could be due to the curvature of the Earth. In the recent study the model is planar. The size of the study area is large enough, that the effect of the curvature could play an important role in the gravity calculation. Therefore the effect of Earth's curvature is investigated in the next step.

2.4 Difference between planar and spherical gravity calculations

In general 3D forward modelling is done in Cartesian coordinates. In order to calculate the effect of the Earth's curvature the gravity effect of a spherical density model has to be calculated and then subtracted from the calculated gravity effect of a planar model. First the Cartesian coordinates have to be transferred into Polar coordinates. A spherical surface can be calculated with (Weisstein, 1999):

$$A = 4\pi|r|^2 = 4\pi\left(\sqrt{x^2 + y^2 + z^2}\right)^2 = 4\pi\left(x^2 + y^2 + z^2\right) \quad \text{(Eq. 2),}$$

whereby the origin of the coordinate-system lays in $x = y = z = 0$ and r is the radius of the sphere. The transformation of Cartesian coordinates into Polar coordinates can be done with:

$$x = r \cdot \cos\varphi \text{ and } y = r \cdot \sin\varphi \quad \text{(Eq. 3)}$$

$$\varphi = \arctan\left(\frac{y}{x}\right) \text{ and } \varphi = \arcsin\left(\frac{y}{r}\right) \quad \text{(Eq. 4)}$$

whereby φ is the angle (clockwise count) and r is the radius of the sphere.

The measured heights h_i of the topography/bathymetry are related orthogonal to the Earth's surface (Figure 19). Therefore the heights can be related to the radius of the Earth R = 6378 km and therefore be transformed (e.g. bathymetry) to a spherical surface by a vector sum with:

$$r_i = R + h_i \quad \text{(Eq. 5)}$$

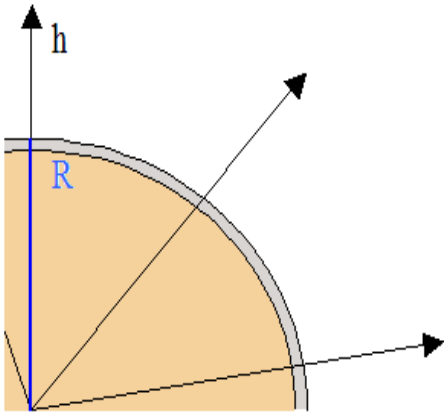

Figure 19 *Vector sum of the measured heights* h_i *on the surface of the Earth and Earth's radius.*

Accordingly the planar layers (Figure 3 till Figure 8) were transformed into spherical layers (Figure 20) by the creation of a sphere with the Earth's radius and the summation of the heights in spherical coordinates. The error, which is made due to the fact that the Earth's shape is not a sphere, is small and can be neglected.
The coordinates are re-transformed to UTM coordinates in order to compare the spherical model with the planar model.

Nowadays no software is available, wherewith the input gravity stations could be placed on a three-dimensional curved surface.
The software GMSYS-2D allows to set the gravity stations on a curved profile. Therefore in the following the gravity effect is calculated along a profile.

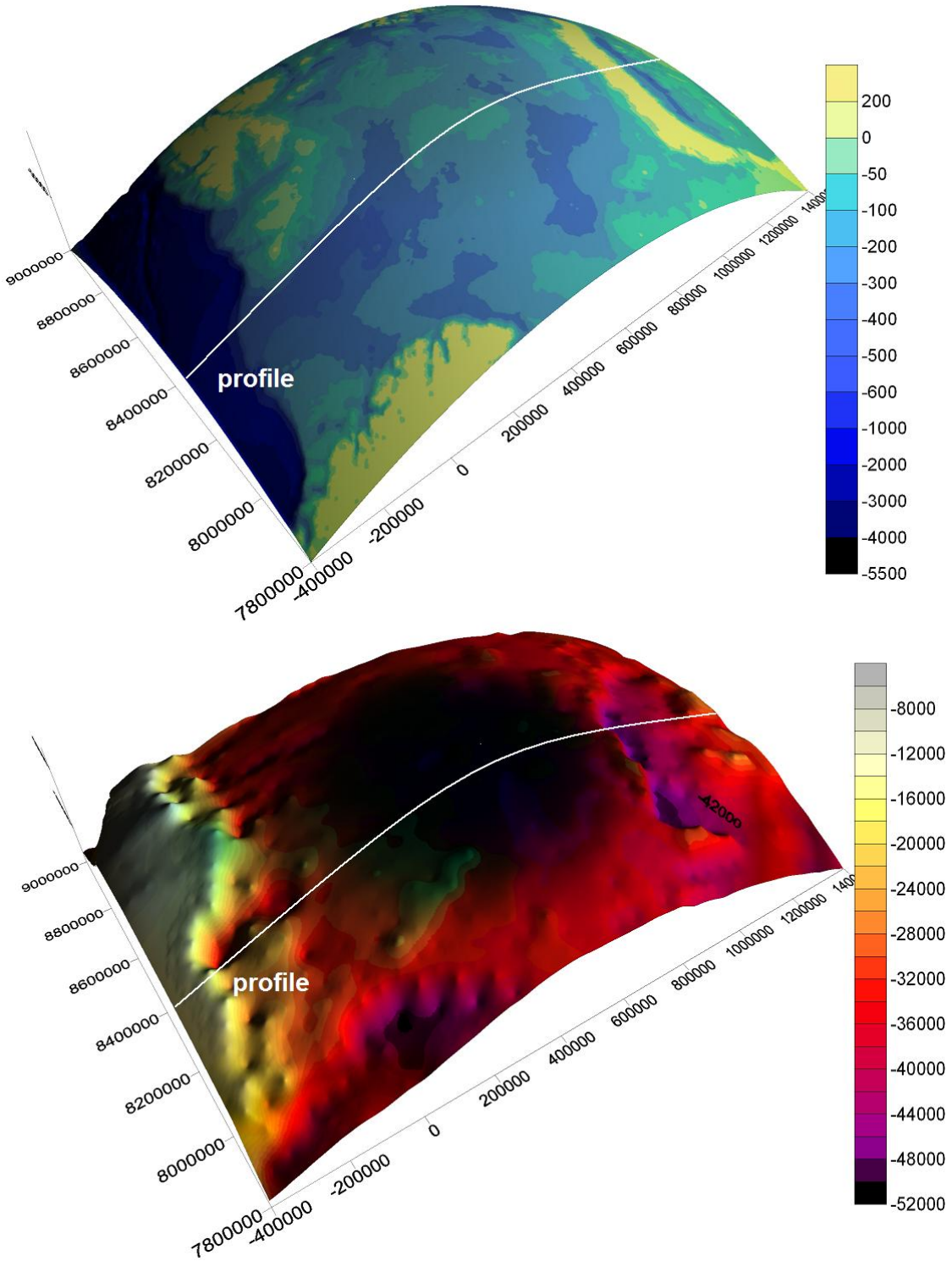

Figure 20 *Spherical layers that were transformed from the planar layers of the 3D density model. Above topography/bathymetry is shown and below the Moho discontinuity.*

The profile strikes parallel to the ordinate from west to east (white line in Fig. 20). The same location was chosen for both the planar layer model and the spherical model. For the planar model the y-coordinate of the profile corresponds to y = 73º in the West and to y = 72º in the East (Figure 21). The gravity stations are remaining planar.

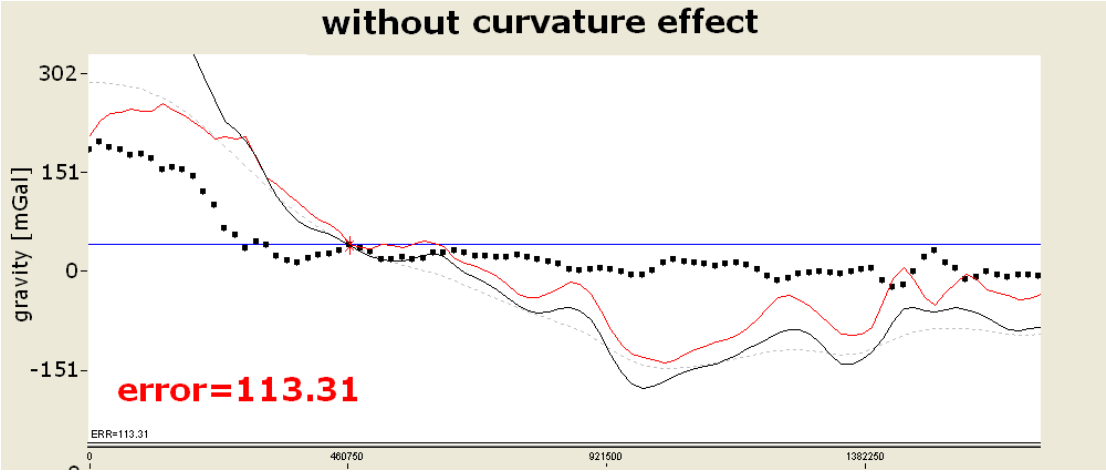

Figure 21 *Calculated gravity (black solid line), observed gravity (black dotted line) and the error (red line) along the profile. Input is the planar density model with flat layers.*

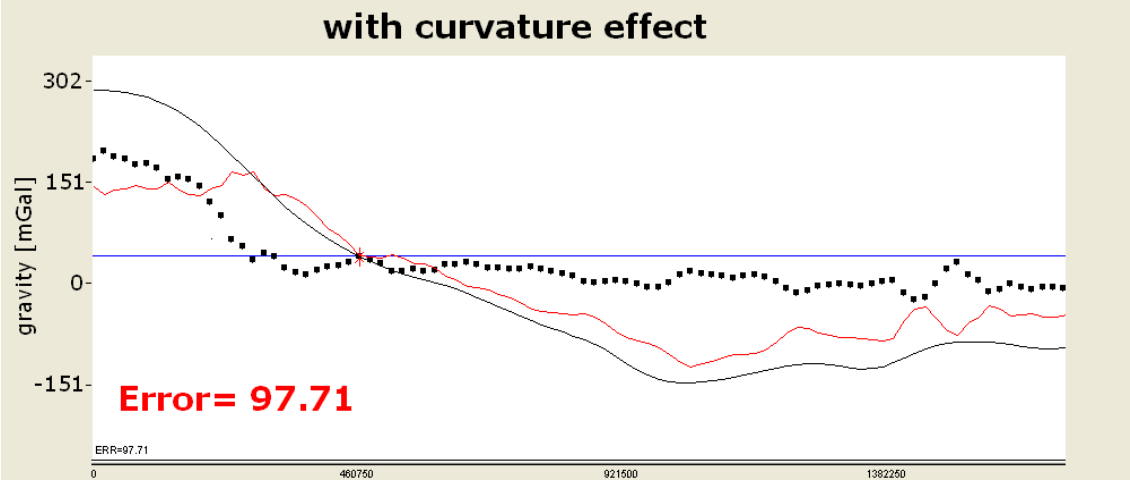

Figure 22 *Calculated gravity (black solid line), observed gravity (black dotted line) and the error (red line) along the profile. Input is the spherical density model with curved layers.*

In the curved-layer-model the profile is located at the coordinate y = 8400000. The input gravity stations are curved as well and were set to the height of the curved water surface (Figure 22). Comparison of the planar and spherical model shows that the spherical model gives a better fit of the observed and calculated gravity. The mean error decreases from 113

$\cdot 10^{-5}$ m/s^2 to 98$\cdot 10^{-5}$ m/s^2.

However, the effect of the Earth's curvature is maximum 15 $\cdot 10^{-5}$ m/s^2 and not enough to adjust the level differences. For this reason isostatic investigations are carried out in the next step.

2.5 Isostatic considerations

In order to investigate the isostatic equilibrium of the crust the external (topography) and internal loading (mass inhomogeneities within the crust) have to be calculated. The load is the product of the density ρ, gravity g and height d:

$$L = \rho \cdot g \cdot d \qquad \text{(Eq. 6).}$$

The load that acts on the Moho was calculated for each layer of the 3D model (Table 2). A Fortran routine was written in order to read the columns of the BARENTS50 model out. Only in 496 columns all density values for all layers (down to Moho) are defined (Table 2).

name of layer	load	number of values	values for same coordinates
water		1169	
upper sediments		1065	
	load of water and sediment		937
lower sediments		1400	
	load acting on basement		937
upper crystalline crust		1416	
mid. crystalline crust		1460	
lower crystalline crust		903	
	load acting on Moho		496

Table 2 *Name of layers and calculated load. The BARENTS50 model is not complete and does not provide a density value for each layer. Accordingly the load that acts on the Moho could only be calculated exactly for 496 columns. The load of the water and upper sedimentary units could be computed for 937 columns.*

In order to calculate the load that acts on the Moho for the entire model, the missing values had to be interpolated. The entire load ranges from 130 $\cdot 10^6$ N/m^2 to 1393 $\cdot 10^6$ N/m^2 with a mean value of 766 $\cdot 10^6$ N/m^2 and a standard deviation of 319 $\cdot 10^6$ N/m^2.

In a last step the load variation compared to the average load (mean value) was calculated in percent (Figure 23). In case the model would be isostatically balanced at the Moho level, only a small variation would be obtained. Due to the fact that a variation from 30-120% is calculated, it can be concluded that the model is not in isostatic equilibrium. In the western part of the study area that is characterized by the ocean-continent transition, the model is isostatically undercompensated. This implies that lower mantle densities would be needed in order to compensate the larger load (compared to the average load of the 3D model). In the eastern and southern part the model is isostatically overcompensated.

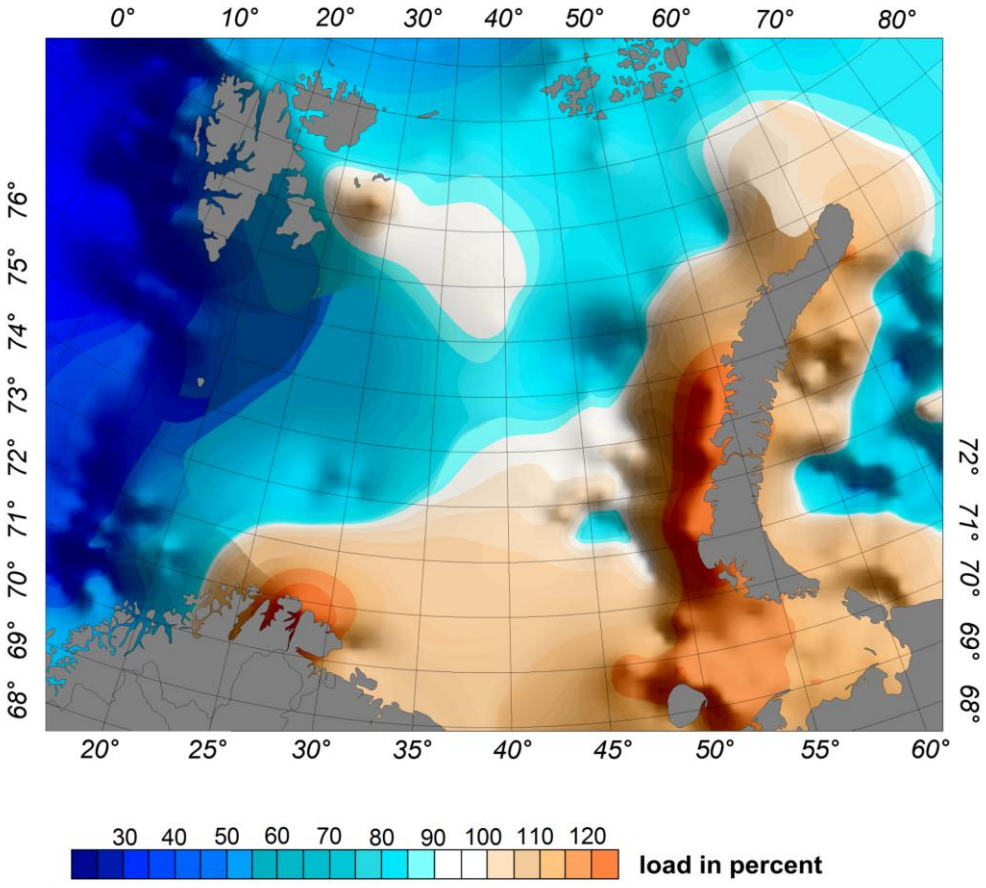

Figure 23 *Load in percent that acts on the Moho surface. The load variation compared to the average load (mean value) was calculated in percent. We obtain a wide variation from 30 till 120 percent, which means that the model is not isostatically equilibrate at the Moho.*

2.5.1 Density variation within the mantle

The following procedure is described by Ebbing and based on the concept of Pratt isostasy (Ebbing et al., 2007). This concept of local isostasy regards the lithosphere-asthenosphere boundary, and not the base of the crust, as the compensation depth balancing the isostatic lithosphere. The chosen lithospheric standard column (crust and mantle) has a reference depth of 120 km and the density distribution according to the Earth reference model (Table 3).

thickness [km]	Density [kg/m^3]	name
12	2670	upper crust
20	2800	middle crust
35	2900	lower crust
120	3250	lithospheric mantle

Table 3 *Earth reference model (after Dziewonski and Anderson, 1981)*

In the following we assume local isostatic equilibrium, which means that the sum of the entire crustal load of the model plus the load of the mantle is equal to the load of the reference Earth model. As result we obtain $961 \cdot 10^6$ N/m^2 for the total crustal load of the reference Earth model. The mean value of the entire crustal load of the 3D density model is $883 \cdot 10^6$ N/m^2. The total lithospheric load of the reference Earth model is $=2710 \cdot 10^6$ N/m^2.

This concept can be expressed by a formula with:

$$\sum_{i=1}^{n} \tilde{\rho}_i \cdot g \cdot (\tilde{d}_i - \tilde{d}_{i-1}) = \sum_{j=1}^{m} \rho_{c,j} \cdot g \cdot (d_{c,i} - d_{c,i-1}) + \rho_m \cdot g \cdot (\tilde{d}_n - d_{c,m}) \quad \text{(Eq. 7)}$$

for $\tilde{\rho}_i$ as density of the reference model, $\tilde{d}_i$ as reference depth, $d_{c,m}$ as moho depth, $\tilde{d}_n$ as lithospheric depth, g as gravity, ρ_m as mantle density and $\rho_{c,j}$ as crustal density.

The isostatic mantle density can be calculated from Equ. 7 with:

$$\frac{\sum_{i=1}^{n} \tilde{\rho}_i \cdot g \cdot (\tilde{d}_i - \tilde{d}_{i-1}) - \sum_{j=1}^{m} \rho_{c,j} \cdot g \cdot (d_{c,i} - d_{c,i-1})}{g \cdot (\tilde{d}_n - d_{c,m})} = \rho_m \qquad \text{(Eq. 8)}$$

The densities of the mantle could be calculated precise for 496 columns. The values ranges from ρ_m= 3181kg/m^3 to 3316kg/m^3 (Figure 24). The mean value is ρ_m= 3240 kg/m^3 with a standard deviation of 31 kg/m^3. The domain of the mantle densities represents realistic density values. As comparison the normal standard value for the mantle density is ρ_m= 3250 kg/m^3.

The density distribution shows the difference between the Eastern and Western Barents Sea. The western part where the ocean-continent transition is located, is characterized by low density values < 3200 kg/m^3 that are associated with the oceanic lithosphere. Medium mantle density values of about 3250-3300 kg/m^3 are prominent in the Western Barents Sea. Higher values > 3300 kg/m^3 are obtained in the Eastern Barents Sea westwards of Novaya Zemlya coincident with the halfmoon-shaped structure in the upper and middle basement (Figure 5, Figure 6).

These calculated isostatic mantle density variations are comparable with the mantle density distribution of the BARENTS50 model (Figure 25) in the western part. However, they are different in the eastern part of the study area. Especially the oceanic lihosphere is characterized by lower values for the isostatic mantle densities.

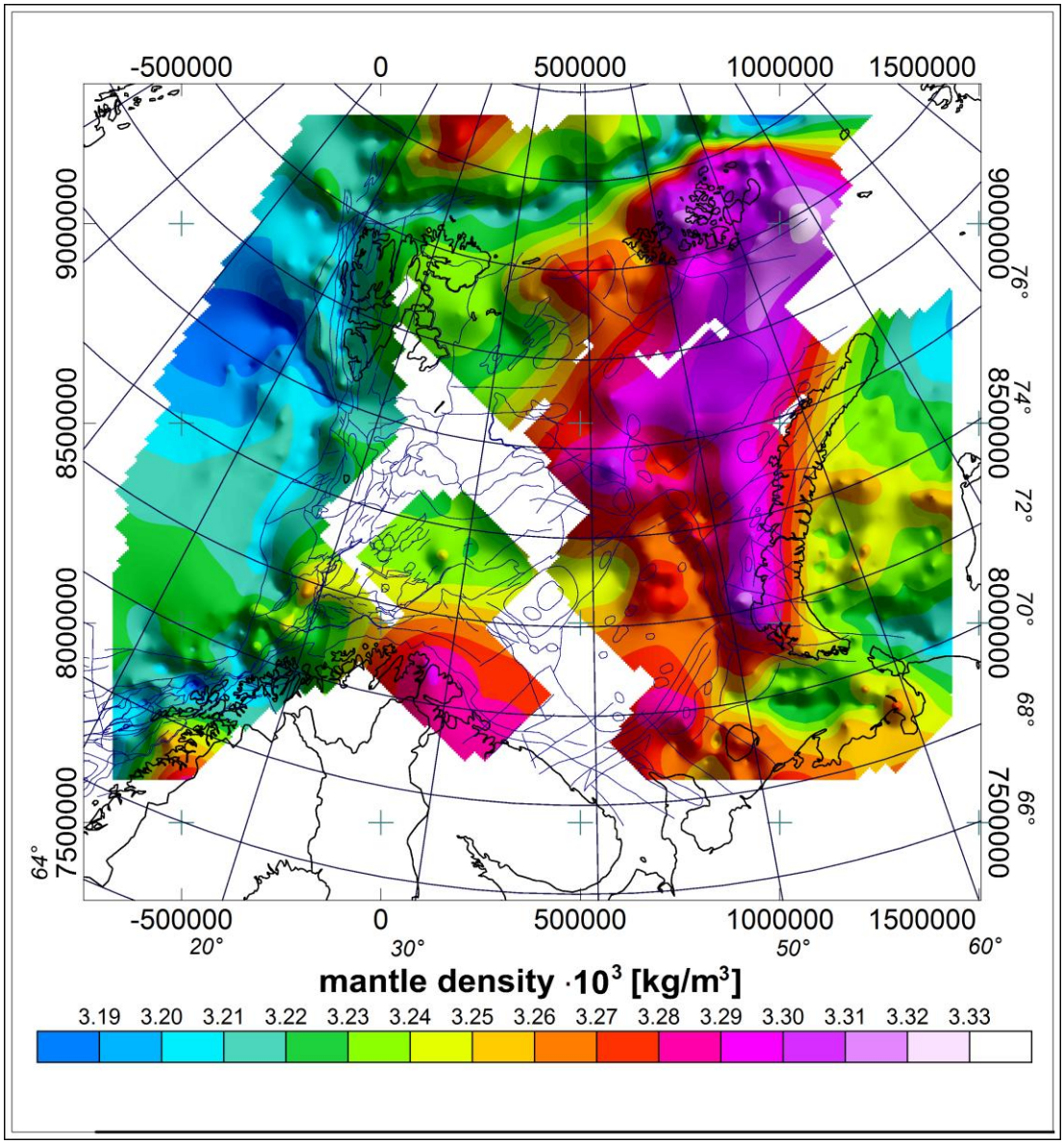

Figure 24 *Density distribution in the upper lithospheric mantle as derived by isostatic calculations.*

The use of the isostatic mantle densities in the 3D density model reduces the discrepancy between the calculated and the observed gravity. However, a misfit is still obtained for the short to intermediate wavelengths in the gravity field. In order to minimize this difference, the density of the lower crust was allowed to vary between 2800-3000 kg/m^3 in the inversion process. This variation produce an gravity field which approximates the observed gravity field (Ebbing et al., 2007).

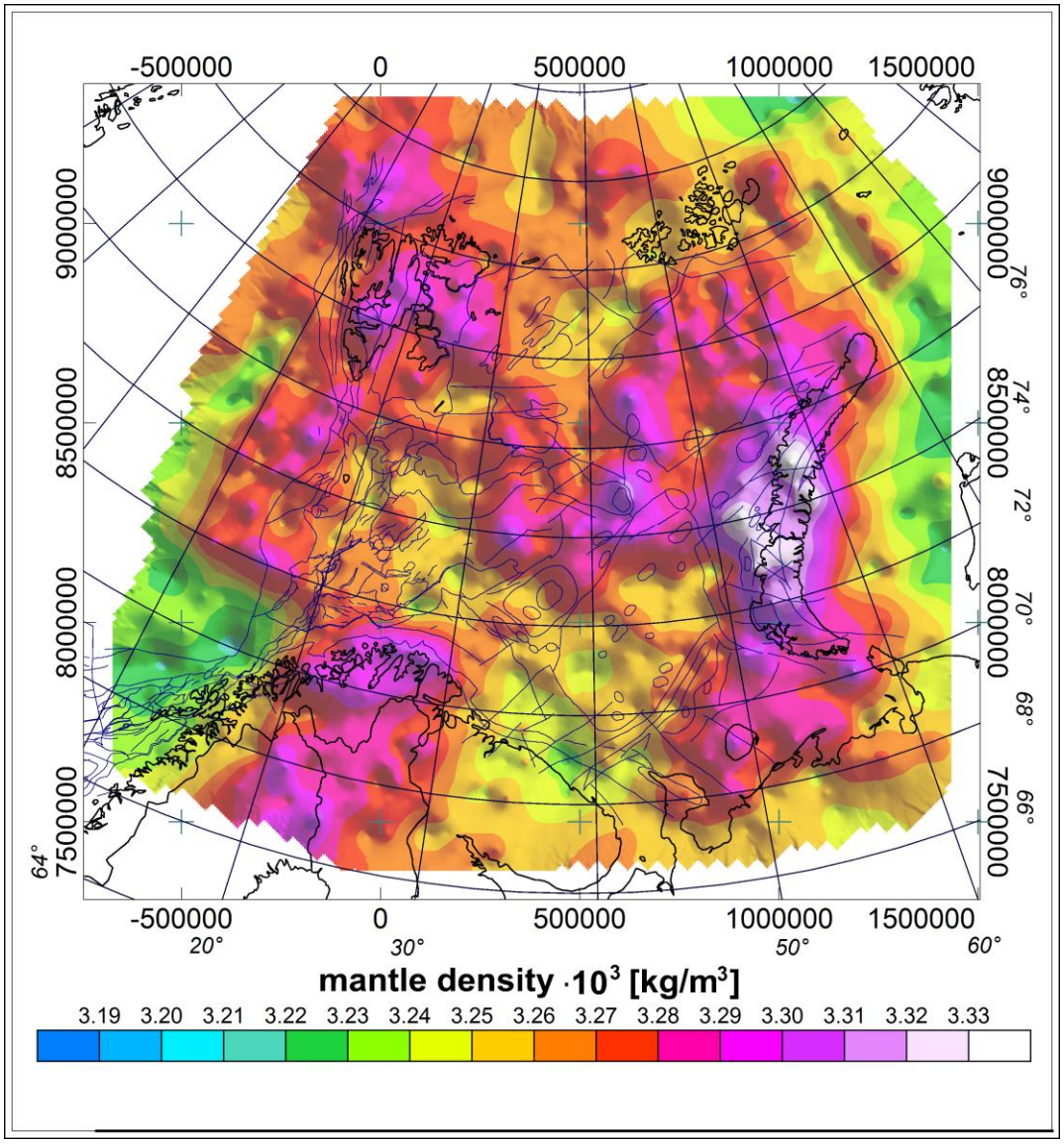

Figure 25 *Density distribution as given from the BARENTS50 model.*

3 RIGIDITY ESTIMATES

The tectonic setting of the Barents Sea is embossed by the Caledonian orogeny (Breivik et al., 2005; Fichler et al., 1997; Gee, 2004; Gudlaugsson et al., 1998). It resulted from the collision of Baltica and Laurentia beginning in Silurian time with duration till the Early Devonian. These two continents were separated by the Iapetus Ocean before the collision event. Accordingly, the orogeny involves the development of subduction systems along the margins of Laurentia and Baltica, and therefore also a tectono-thermal history. The geological and tectonic history is complex and characterized by magmatism, sedimentation, deformation and metamorphism, which was an essential part of the Early Caledonian evolution.

Such a tectonically history is supposed to left its signature within the crust and lithosphere. It was already shown that the locations and directions of faults and tectonically units correlates with the areas of a rapid change of the elastic thickness or flexural rigidity values (Wienecke, 2006; Wienecke et al., 2007). For this reason it is proposed that the location of the Caledonian (Scandian) sutures and deformation front is visible in the elastic thickness/ flexural rigidity distribution. In the following the notations "Te" for the elastic thickness and "D" for the flexural rigidity will be used. The software LithoFLEX (Braitenberg et al., 2007) provides a tool for D and Te calculation.

3.1 Input data

The 3D model was used to compute the entire load from all layers: top sediments, lower sediments, top basement, middle basement, lower basement. All lateral and horizontal density variations are included.

3.2 Moho

As reference Moho the modelled Moho from the 3D model is used (Figure 7 and on the left side in Figure 29). The Moho varies over large parts of the Barents Sea region between 32.5 and 37.5 km. The main changes can be related to the Svalbard-transition and the onshore/offshore transition in the south. Generally, the Moho is relatively flat and does not show a correlation with the top basement geometry (Ebbing et al., 2007), as it would be

expected from simple isostatic models of crustal extension (McKenzie, 1978). From the view of isostasy is this an indicator for a change in the physically properties of the lithosphere. Accordingly the Moho geometry should be explainable with a change in the elastic thickness or flexural rigidity, respectively.
In order to investigate the tectonic settings in the Barents Sea in more detail, we use the analytical solution for an elastic plate (Wienecke, 2006; Wienecke et al., 2007) to calculate the Te/D distribution in the greater Barents Sea region.

3.3 Calculation of flexure Moho

The classical concept of regional isostasy after Vening-Meinesz proposes that the flexural strength of the lithosphere has to be taken into account for isostatic consideration. The resulting flexure of a thin plate can be described by 4th order differential equation. In the past the problem has been dealt with in the field of frequency space, where the equation was solved with Fourier transformation techniques (e.g. coherence and admittance). However, the spectral approach has some drawbacks, making the results disputable. Wienecke (2006) retrieved one unified **A**nalytical **S**olution for the **E**lastic **P**late (ASEP). The ASEP is used for computation of the flexural crust mantle interface. Thereby the input grid contains information about the topographic load as well all internal load variations. These internal load variations are given by the density variations from the 3D density model. The internal load variations can be taken into account with the ASEP (Wienecke, 2006). The Moho that is calculated with the ASEP is in the following referred to as "Flexure-Moho".

The flexure Mohos were calculated with the parameter: grid node distance $dx = dy$ = 5 km, reference depth = 30 km, density contrast $\Delta\rho$ = 400 kg/m^3 (for density of lower crust ρ_c = 2900 kg/m^3 and density of upper mantle ρ_m = 3300 kg/m^3), ΔTe = 1 km, whereby Te range from 1 km to 65 km.
The maximal radius of convolution was set to R = 200 km, accordingly the error in the deflection value of the flexure Moho is = 10 %.

3.3.1 Comparison of analytical calculation with Airy isostasy

The Moho undulation, which we obtain from the Airy isostasy (Figure 26) is compared to

the flexure Moho that was calculated with the ASEP for a reference depth of 30 km, an elastic thickness value Te = 0.9 km and a constant Young's modulus of E = 100 GPa (Figure 27). In theory both boundaries should be similar, since the deflection values of the flexure Moho has to converge to the Airy isostatic case for small Te values (Wienecke, 2006).

The Moho for the Airy isostasy and the flexure Moho are very similar in depth values and in the regional behaviour in the eastern part with deepening under Novaya Zemlya and the upwelling due to the ocean-continent transition in the western part of the study area. The calculation of the flexure Moho's for another Young's modulus of E = 10 GPa shows similar results. For example the Moho depth of the flexure Moho for Te = 0.9 km are in the range of –41 and –24 km, which is a difference of less than 1 km compared to the depth values for the calculation with E = 100 GPa.

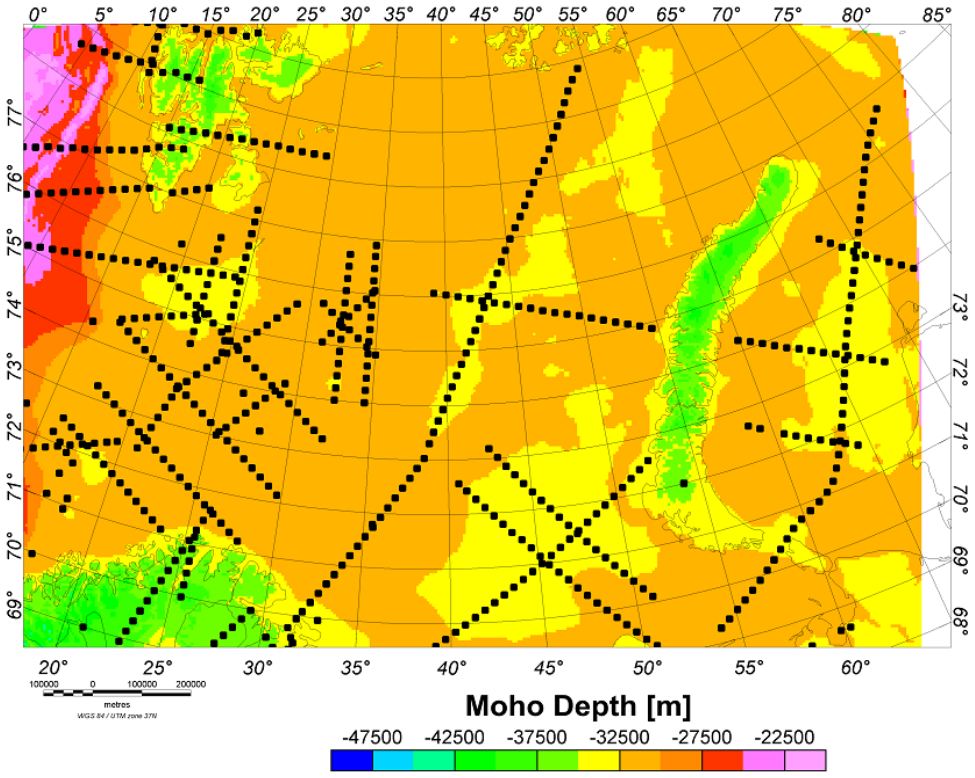

Figure 26 *Moho calculated for the Airy isostatic case with Fast Fourier transformation techniques for bathymetry and sediment load (Ebbing et al. 2007).*

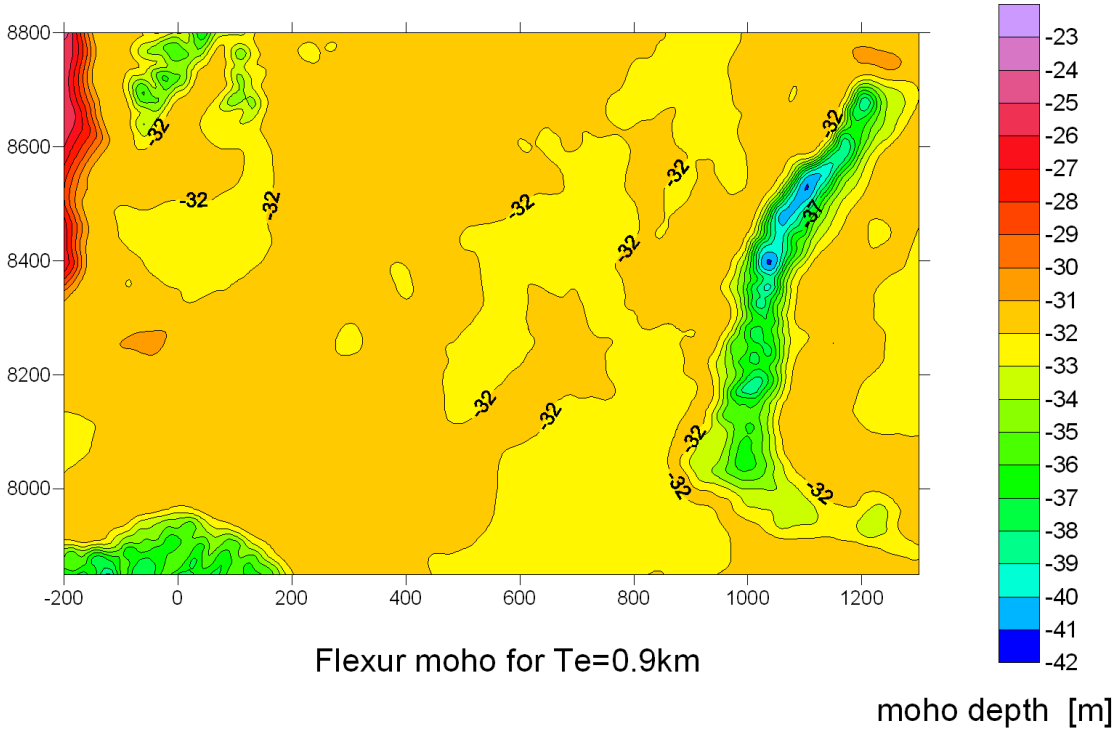

Figure 27 *Moho calculated with the ASEP for Te=0.9 km and reference depth 30 km.*

The large Moho depth of –52 km cannot be reproduced for a reference depth of 30 km with the flexural approach. In order to do so a value of the Young modulus of $E < 0.01$ GPa would be needed, which is unrealistic.

The only possibility to reproduce the deep root under Novaya Zemlya is to use another value for the reference depth of 40 km. In Figure 28 two different flexure Mohos for the elastic thickness values Te = 1 km and Te = 15 km are shown. The Moho depth values expected from the Barents50 model in the area around Novaya Zemlya can be approximated with this reference value. However, the Moho depth values of the Eastern and Western Barents Sea can not be reproduced with a reference depth of 40 km. The correct choice of the reference depth is essential for the elastic thickness calculation and was investigated by Wienecke (2006).

In the following we will calculate the elastic thickness/flexural rigidity distribution for both reference depths of 30 and 40 km.

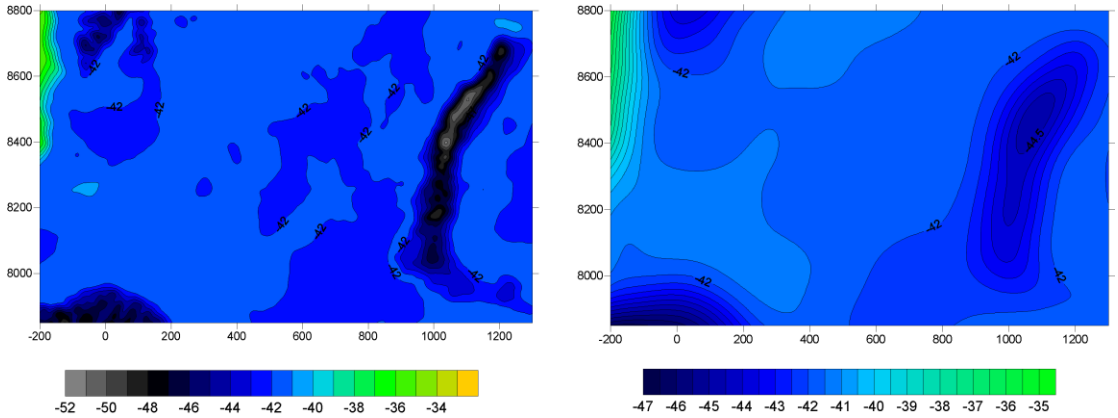

Figure 28 *Moho calculated with the ASEP for a reference depth of 40km and various elastic thickness values. Left side: Te=1km. Right side: Te=12km.*

In addition it is worth to mention that the gravity potential field modelling set an upper limit for the Moho depth with 45 km (pers. comm. Ebbing). Another important fact is, that in the region of Novaya Zemlya no receivers were positioned on land, accordingly the seismic profiles have no data coverage in this region (pers. comm. J. - I. Faleide). As a consequence, the root beneath Novaya Zemlya is not constrained in the BARENTS50 model. The comparision of the reference Moho derived from the BARENTS50 velocity model and the results of the Airy isostatic calculations shows a large difference. In the next step we further investigate the reference Moho and compare it with the flexure Moho that was calculated with the ASEP.

3.3.2 Comparison with Reference Moho

For first investigation, a flexure Moho was calculated for a constant elastic thickness value of *Te* = 12 km and a reference depth of 30 km with the analytical solution for an elastic plate (ASEP). Thereby the elastic thickness value *Te* = 12 km represents a standard value for the crust. This flexure Moho is approximate but is already comparable with the reference Moho from the BARENTS50 model in terms of its geometry and undulation (deepening below Novaya Zemlya and upwelling at the western margin of the study area). However, in order to achieve a local fit to the reference Moho we must vary the Te values. Vice versa, by comparison of the calculated flexure Moho (for each Te value) with the reference Moho we can obtain the Te distribution (Braitenberg et al., 2006; Wienecke et al., 2007). This is done with the software LithoFlex (Braitenberg et al., 2007).

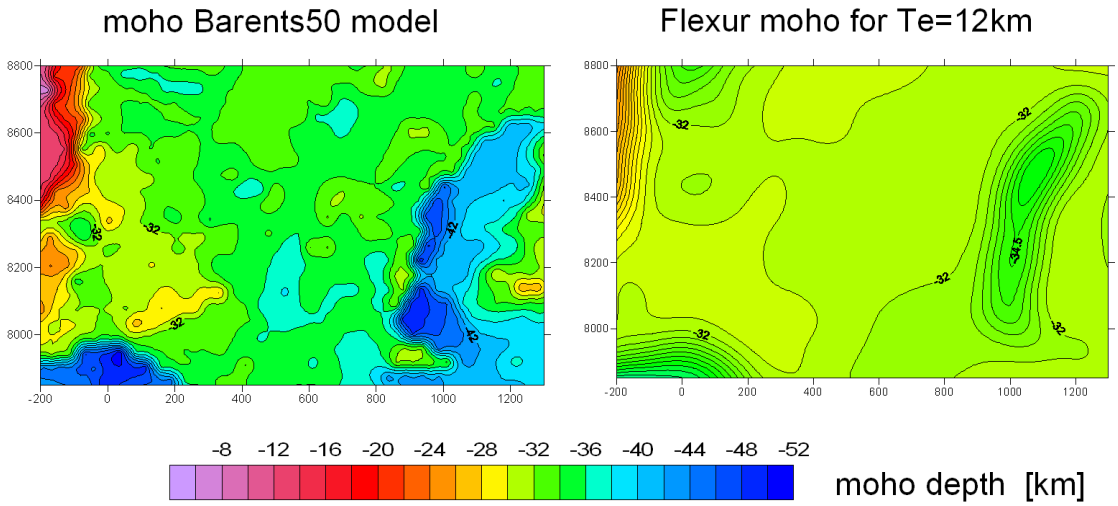

Figure 29 *Left side: Moho from the BARENTS50 model. Right side: Flexure Moho calculated with the ASEP for Te=12 km and a reference depth of 30km.*

The comparison of the flexure Moho for Te = 12 km calculated for the reference depth 40 km (Figure 28) shows that the deep root of Novaya Zemlya can be reproduced. However, the Moho depths of the entire study area can not be explained with this reference depth.

3.4 Inversion of elastic thickness

A set of flexure Mohos for a range of rigidity values $D = 8.89 \cdot 10^{18}$ Nm to $2.44 \cdot 10^{24}$ Nm has been calculated, which corresponds, for the Poisson ration $\nu = 0.25$ and the Young's modulus E = 100 GPa, to the elastic thickness values Te = 1 km to 65 km. Each flexure Moho corresponds exactly to one flexural rigidity value. Hence, the comparison of the computed flexure Mohos with a reference Moho over an area with a given side length L provides one constant rigidity value for this subsection, resulting in a high spatial resolution of the flexural rigidity distribution. The comparison of the flexure Mohos with a reference Moho is done by the choice of the minimum root mean square (RMS) value (Braitenberg et al., 2006).

The inversion of the elastic thickness was done for both reference depth values. The RMS value distribution gives information about the precision of the calculation. A low RMS value < 1 means a very good fit between the flexure Mohos and the reference Moho and a very good precision of the resulted elastic thickness inversion (white color in Figure 30). A

RMS value <5 means a good fit and a good precision of the result (blue colour in Figure 30). For a RMS value of >10 the result is questionable (yellow colour in Figure 30). Comparison of the RMS value distribution for both reference (Figure 30) depth shows that for 30 km the calculation is precise. The RMS value is <5 in the area of Eastern and Western Barents Sea. In the area of Novaya Zemlya the RMS values are <10, therefore the results of the elastic thicknes distribution are not precise but can be still taken into account. However, in this part of the study area further investigations are needed.

For a reference depth of 40 km the RMS values are in general higher than 5, only in the area of Novaya Zemlya, smaller values <5 are obtained. The results of the elastic thickness inversion for a reference depth of 40 km have therefor not a good precision and would be questionable. In addition, the deep root of Novaya Zemlya was not constrained by a seismic station in the Barents50 model, and also from the potential field modelling the high depth values were questionable (see Chapter 3.3.1).

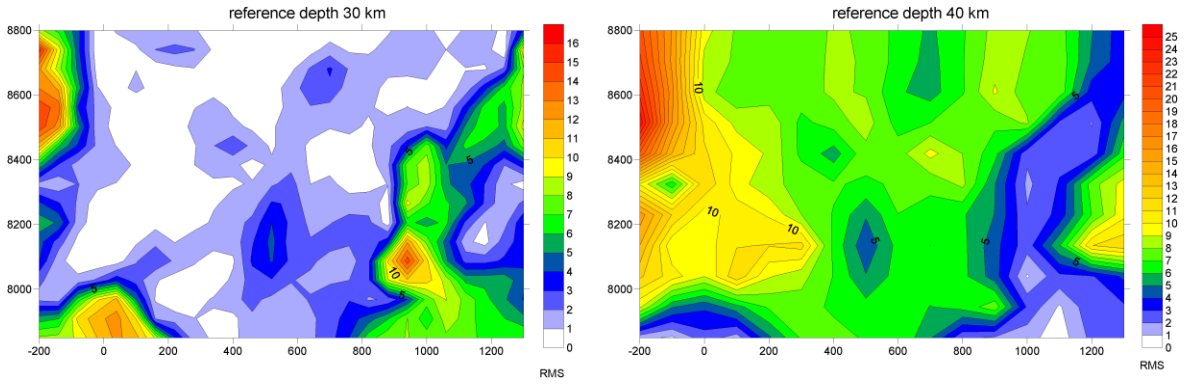

Figure 30 *RMS value distribution of the elastic thickness inversion for two different reference depth values. Left side: 30 km. Right side: 40 km.*

Therefore we prefer the results of the elastic thickness inversion for the reference depth of 30 km. The resulted elastic thickness / flexural rigidity distribution for a reference depth of 30 km in the Barents Sea shows a clear evidence for a large difference between the Eastern and Western Barents Sea (Figure 31). The Svalbard transition, the western part and Novaya Zemlya are characterized by low values, which indicate a weak crust.

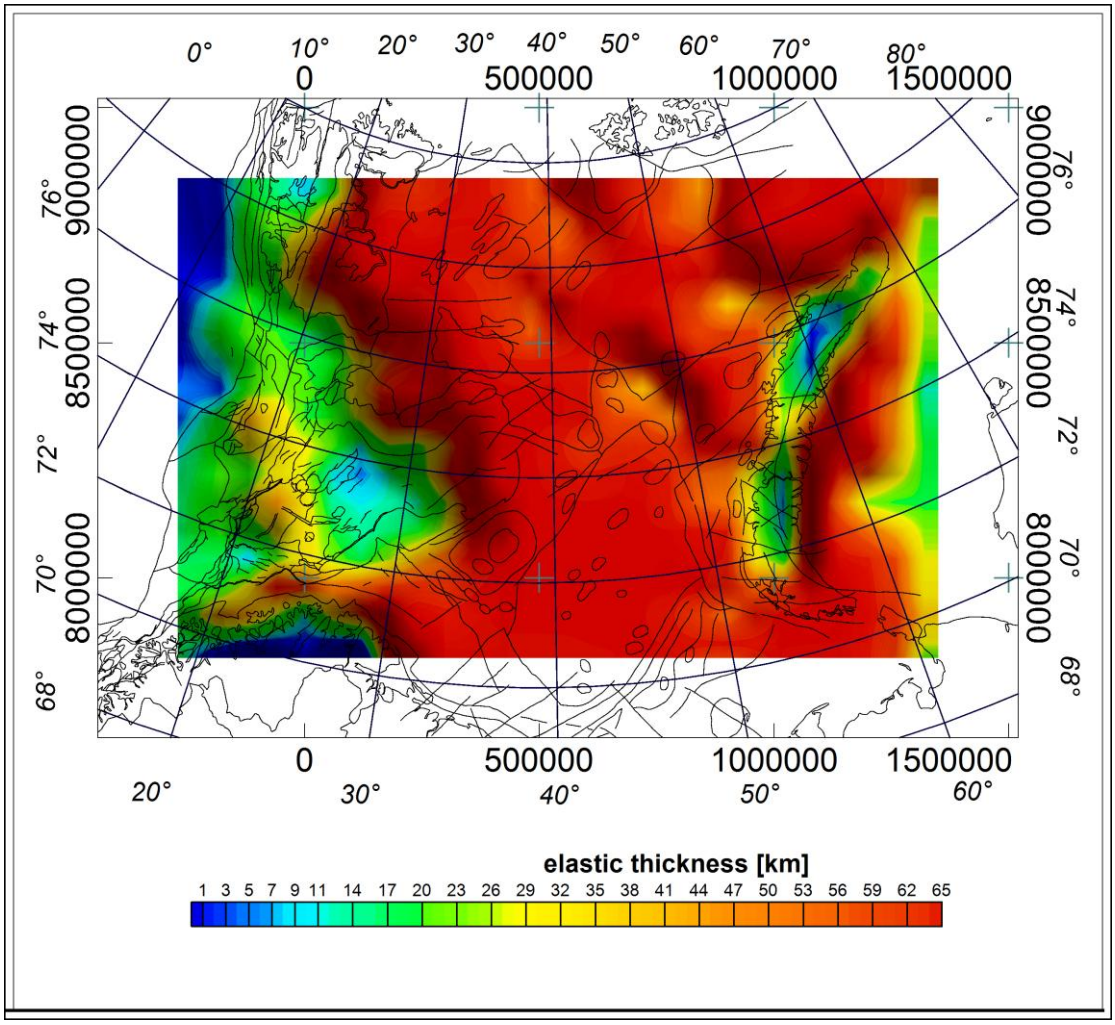

Figure 31 *Elastic thickness / flexural rigidity distribution in the Barents Sea. The Svalbard transition, the western part and Novaya Zemlya are characterized by low values, which indicate a weak crust. In the middle part of the study area high Te values were obtained.*

High Te values >55km were obtained in the middle part of the study area. This indicates a rigid crust and should correlate with higher p-wave velocities.

Seismic tomography (Faleide et al., 2006) detected a high-velocity structure in the lithospheric mantle below the Eastern Barents Sea located between Novaya Zemlya and the Eastern-Western Barents Sea transition zone with its western boundary having a bending parallel to Novaya Zemlya. This area is also correlating with the area of higher mantle densities (Ebbing et al., 2007). An overlay with tectonical/geological structures was done by Torsvik (pers. comm.) in comparison with the results from seismic and mantle density studies to give a preliminary interpretation of the results (Figure 32 - Figure ***34***).

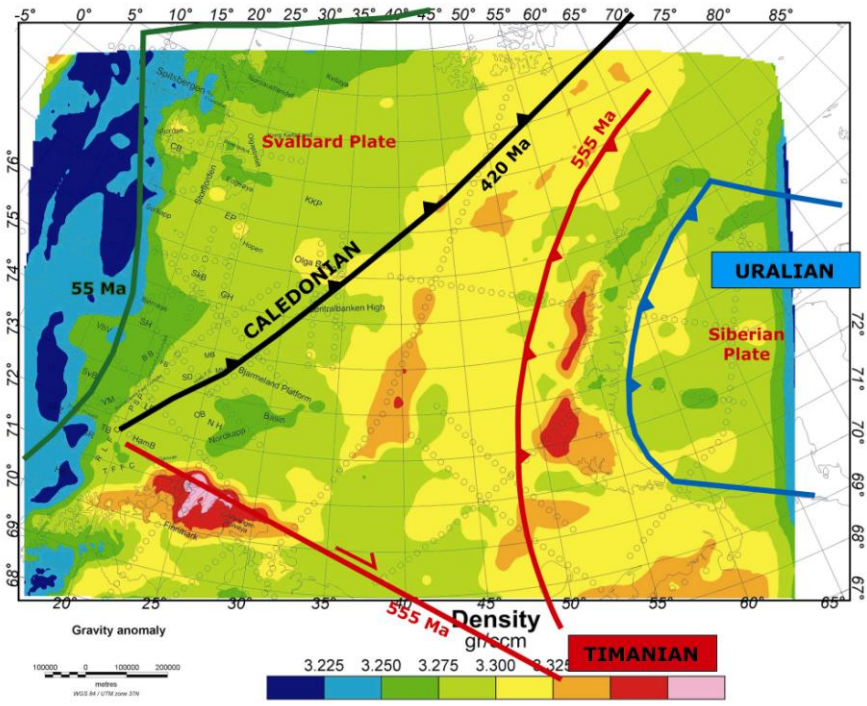

Figure 32 *Mantle density distribution from isostatic calculated mantle densities with an overlay of tectonic interpretation by T. Torsvik (pers. comm.). Higher mantle densities are obtained in the middle part of the study area and in the foreland basins of Novaya Zemlya.*

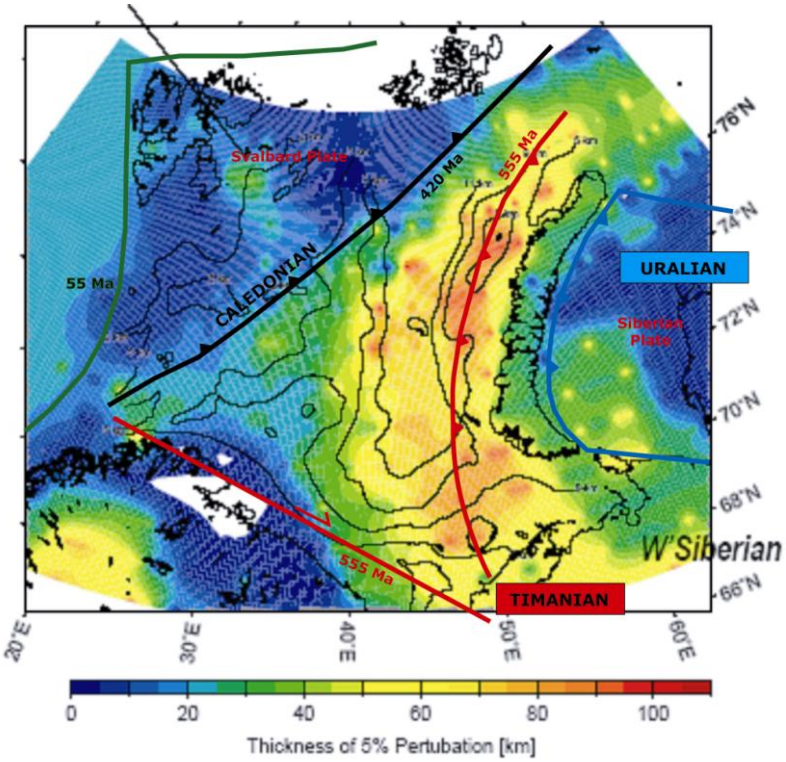

Figure 33 *Thickness of velocity pertubation resolved by mantle tomography (Faleide et al., 2006, Levshin et al., 2007), the structure is deepening below Novaya Zemlya. Overlay of tectonic elements by T. Torsvik (pers. comm.).*

The Uralian trend can be seen in the mantle density distribution, the tomography model and in the elastic thickness distribution (marked with blue line). However, the elastic thickness distribution does not correlate with the location of the proposed Caledonian trend (marked by black line), in contrast to the results of the mantle density distribution and the seismic tomography observation. As well there is no correlation of the Timanian trend with the Te distribution. Therefore we refine our results by applying a new theory of an equivalent elastic thickness (Wienecke et al. 2007), which will be introduced in the following.

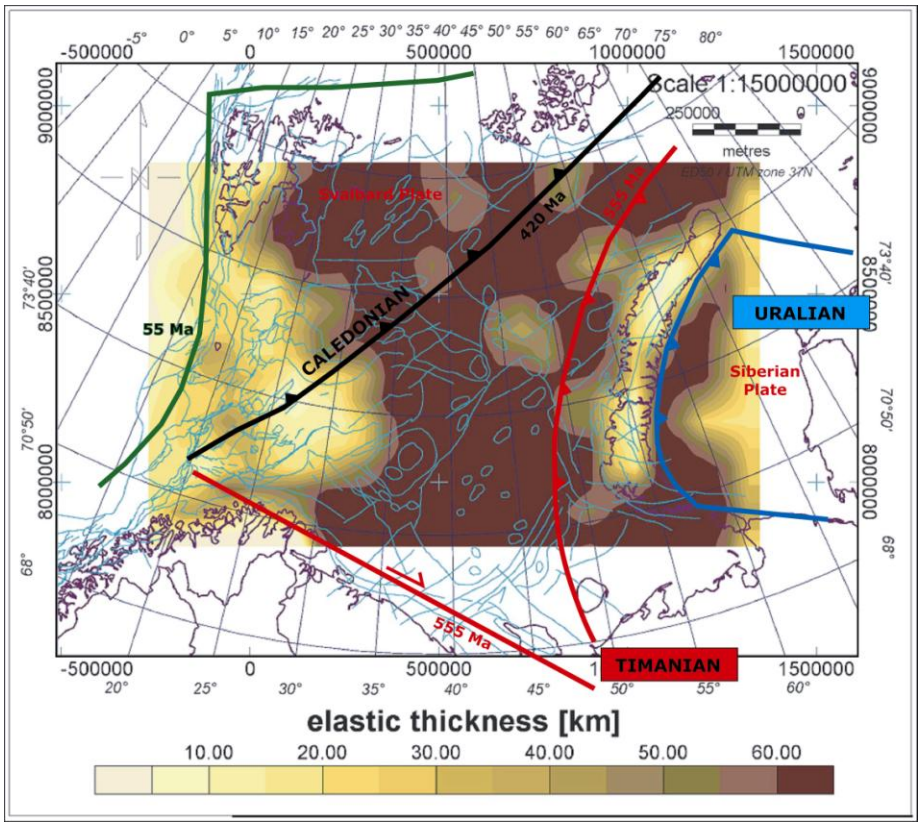

Figure 34 *Elastic thickness /flexural rigidity distribution with an overlay of tectonic interpretation by T. Torsvik (pers. Comm.).*

3.5 Equivalent elastic thickness

In the past the elastic thickness has been used synonymously for the flexural rigidity, since it was defined by the material parameters of Young's modulus and Poisson ratio, which were assumed to be constant. The application of the ASEP shows, that it is sufficient to operate with a constant value for the Poisson's ratio, as the variation does not lead to a significant change in the results (Wienecke 2006). However, concerning the vertical and

horizontal variations in crustal composition, which corresponds to a change of Young modulus by orders of magnitude - the use of a constant standard value in the calculation process is doubtful. For that reason the Te distribution was recalculated including the Young's modulus variation, which could be estimated by using the P- wave velocities of the Barents50 model.

This work is described by Wienecke *et al.* and is related to the theory of the elastic thickness (Wienecke et al., 2008, in preparation).

The parameter that characterizes the apparent flexural strength of the lithosphere is the flexural rigidity D, which is defined with the material parameters Young's modulus E, the Poisson's ratio ν and the elastic thickness T_e with the following equation:

$$D = \frac{E \cdot T_e^3}{12(1-\nu^2)} \qquad \text{(Eq. 9)}$$

Therefore, if one refers to Te instead of D, one implies a choice of a rheological model. Recently, standard values are used in the literature with $E = 10^{11} Pa = 10^{11} Nm$ and $\nu = 0.25$ (Burov and Diamont 1995). The ASEP is not sensitive to a change of Young's modulus, because 100% deviation of E causes 30% deviation of the deflection w_0. However, the parameter of Young's modulus is not exactly estimated. Generally a standard value of $E = 10^{11} Pa$ is used in the calculation. The Earth Reference Model proposed by Dziewonski and Anderson gives an average pressure-value of 0.2 kbar at 3 km depth, 3.3 kbar at 15 km depth, 6 kbar at 25 km depth and 11 kbar at a depth of 40 km (Dziewonski and Anderson, 1981).

The Young's modulus was measured by Christensen for different rock types at similar pressure conditions for 0.2, 4.0, 6.0 and 10.0 kbar (Christensen, 1978). The results show a variation of the values around 40-160 GPa (see Figure 35). Accordingly, an inaccuracy of the Young's modulus of >50 % is probable. This leads to a high error in the calculation of the deflection. Hence, the Young's modulus variation should be taken into account in the calculation of the flexural rigidity distribution.

At the present time there is no formula known in order to take the vertical and horizontal variation of Young's modulus into account. It is not clear, if it is allowed from the physically point of view to calculate a simple average. A new formula has to be derived in

order to calculate the effective Young's modulus for a horizontal and vertical variation.

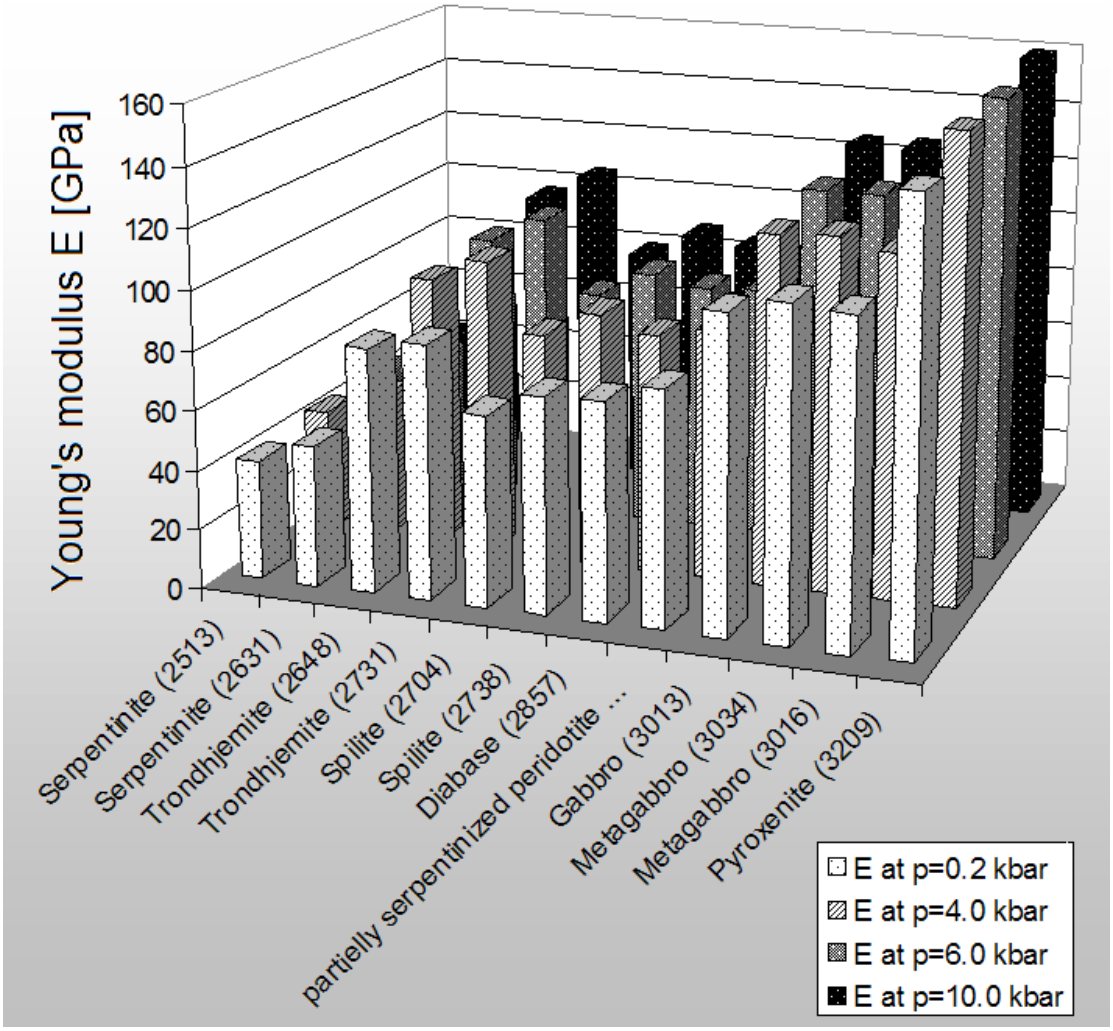

Figure 35 *Shown are the Young' s modulus values measured by Christensen (1978) for different rock types at various pressure conditions. Numbers in the brackets besides the rock type give the average density value in kg/m^3. There is obviously a variation of the Young's modulus ranging from 40 to 160 GPa.*

3.5.1 The effective Young's modulus for a layered body

We consider a body that consists of a matrix with a Young's modulus E_M. Within the matrix are different layers with different thickness, but with the same Young's modulus E_L. We assume that E_L is larger than E_M. First, we derive a mathematical description for a simple case. Later we extend this formula for layers with a varying Young's modulus. Two boundary cases (Ashby and Jones, 2005; Föll, 2007) are considered in the following.

Case A: stress applied parallel to the layer

The strain ε is equal for each cross sectional area (shown by Föll 2007 based on e.g. (Ashby and Jones, 2005)). In order to stretch the layer with the larger Young' modulus, the force applied on a cross sectional area is larger compared to an equal area for the matrix. Consequently the stress σ must vary (Figure 36).

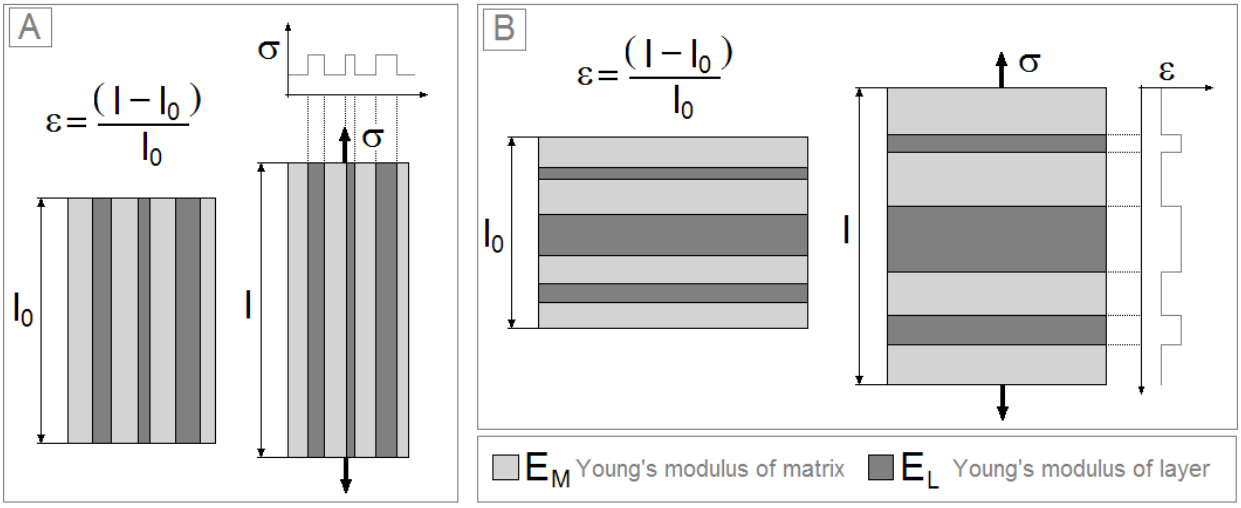

Figure 36 *Two-dimensional consideration of a material with fibers, which consist of different young modulus related to the matrix, left side: stress applied parallel to the fibers, right side: stress applied oblique to the fibers.*

For the equal strain $\varepsilon = \varepsilon_L = \varepsilon_M$ and according to Hook's law, the stress of the layers ε_l and the matrix ε_m can be written as:

$$\sigma_L = E_L \cdot \varepsilon \qquad \text{(Eq. 10)}$$

and

$$\sigma_M = E_M \cdot \varepsilon \qquad \text{(Eq. 11).}$$

The total force F that acts on the entire area is:

$$F = F_M + F_L = \sigma_M \cdot A_M + \sigma_L \cdot A_L \qquad \text{(Eq. 12).}$$

For the effective stress follows:

$$\sigma_{eff} = \frac{F}{A} = \frac{\sigma_M \cdot A_M + \sigma_L \cdot A_L}{A} = \sigma_M \cdot \frac{A_M}{A} + \sigma_L \cdot \frac{A_L}{A} \qquad \text{(Eq. 13).}$$

With Eq. 10 and 11 follows:

$$\sigma_{eff} = E_M \cdot \varepsilon \frac{A_M}{A} + E_L \cdot \varepsilon \frac{A_L}{A} = \varepsilon \cdot \left(E_M \cdot \frac{A_M}{A} + E_L \cdot \frac{A_L}{A} \right) \qquad \text{(Eq. 14).}$$

According to Hook's law the term in the brackets is the expression for the effective Young's modulus, with:

$$E_{eff} = E_M \cdot \frac{A_M}{A} + E_L \cdot \frac{A_L}{A} \qquad \text{(Eq. 15).}$$

Case B: stress applied oblique to the layer

In this case the stress σ is equal for each cross sectional area (Figure 36). The layers will be less expanded than the matrix. For this reason the strain ε must vary. The total strain is related to the sum of the expanded areas with:

$$\varepsilon = \frac{A_M \cdot \varepsilon_M}{A} + \frac{A_L \cdot \varepsilon_L}{A} \qquad \text{(Eq. 16).}$$

As a result of Hook's law we obtain:

$$\varepsilon = \frac{A_M \cdot \sigma}{A \cdot E_M} + \frac{A_L \cdot \sigma}{A \cdot E_L} \qquad \text{(Eq. 17).}$$

Thus gives for the effective Young's modulus:

$$E_{eff} = \frac{1}{\frac{A_M}{A \cdot E_M} + \frac{A_L}{A \cdot E_L}} \qquad \text{(Eq. 18).}$$

For both boundary cases a formula for the effective Young's modulus is found, which can be extented to a horizontal and vertical Young's modulus variation (Wienecke et al., 2007,

in preparation). These formulas are identical to the formulas of the total resistance in case of serial and parallel connexion according to the principles of electrical engineering. This is not by accident, but a consequence of a similarity of Hook's law with Ohm's law for voltage U, resistance R and current I:

$$U = R \cdot I \qquad \text{(Eq. 19).}$$

These two laws are not only mathematically similar, but also from the physically point of view: A driving force causes an answer. The cause and the effect are related to each other in a linear way. Accordingly, we can apply the derived formula also for various layers, similar to the principles of electrical engineering for many resistances.
Therefore it follows for the boundary case B:

$$E_{eff} = \frac{1}{\frac{A_1}{A \cdot E_1} + \frac{A_2}{A \cdot E_3} + \ldots \frac{A_M}{A \cdot E_M}} \qquad \text{(Eq. 20).}$$

For the 3D case the relative volume V_i/V instead of the relative area A_i/A has to be used (Wienecke et al., 2007, in preparation).

3.5.2 The effective Young's modulus in the Barents Sea region

The seismic velocities from the BARENTS50 model were used in order to estimate the Young's modulus variation E_i within each layer for each density value ρ_i. The P-wave velocities $v_{p,i}$ are related to the Young's modulus with:

$$E_i = v_{p,i}^{\,2} \cdot \rho_i \cdot \frac{(1-2\nu)(1+\nu)}{(1-\nu)} \qquad \text{(Eq. 21).}$$

for the Poisson's ratio ν=0.25. The BARENS50 model has a resolution of dx = dy = 50km. The hight h is given by the depth or thickness of each layer. For the relative volume V_i / V with $V_i = dx \cdot dy \cdot h_i$ the height h_i is related to the entire height of the model, which corresponds to the Moho depth. The derived formula was applied to the Barents Sea. Per column the effective Young's modulus vertical and horizontal was calculated (Figure 37).

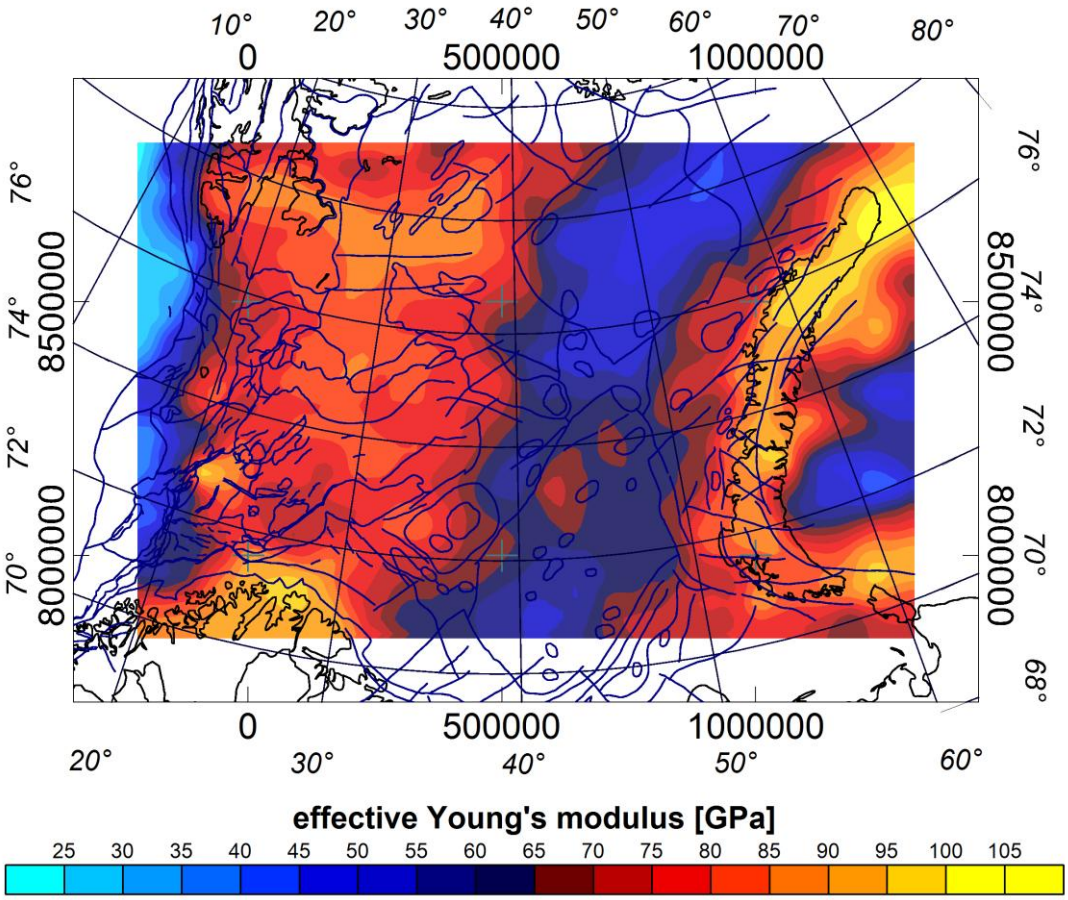

Figure 37 *Effective Young's modulus variation (vertical and horizontal) in the Barents Sea.*

The distribution of the effective Youngs modulus ranges from 25 to 105 GPa. Low values are obtained at the western margin coinciding with the oceanic crust. The area of Finnmark, Svalbard and Novaya Zemlya is characterized by high values.

In general the difference between the Eastern and Western Barents Sea is clearly shown by the effective Young's modulus distribution. The western part is characterized by intermediate values of ca. 70 - 85 GPa. In contrast to this is the eastern part westwards and eastwards from Novaya Zemlya represented by low values < 65 GPa. The Te distribution was recalculated including the Young's modulus variation, which gives the equivalent elastic thickness (Figure 38, on the right side). The elastic thickness distribution calculated with the ASEP and constant Young's modulus 100 GPa shows almost no variation in the middle part of study area. The elastic thickness distribution calculated with the ASEP and Young's modulus variation shows almost high elastic thickness values variation in the middle part of study area.

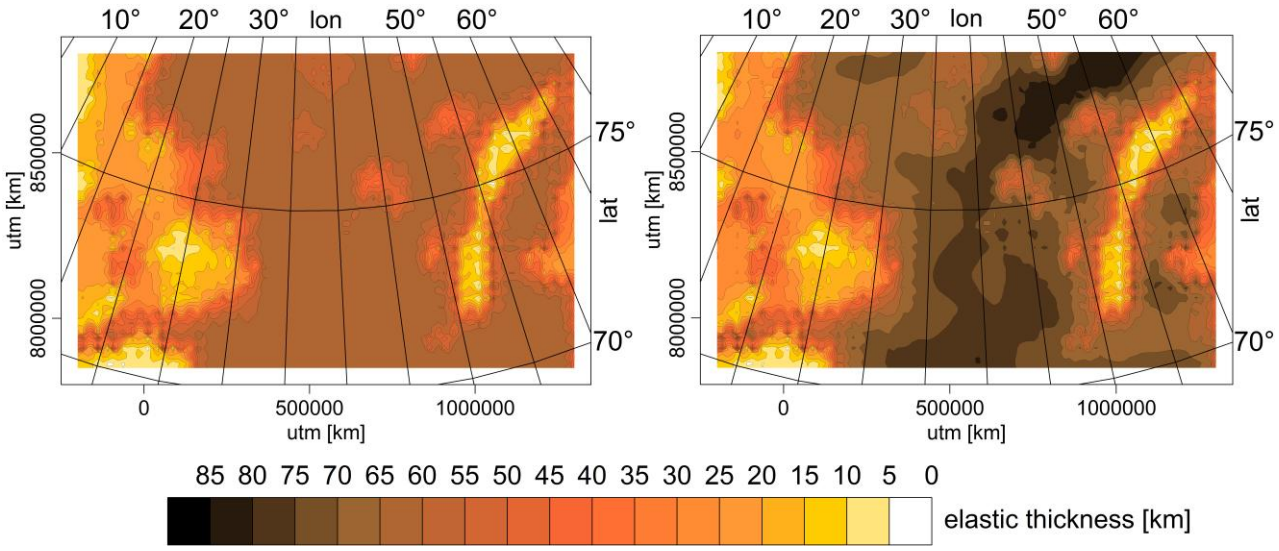

Figure 38 *On the left side: elastic thickness distribution calculated with the ASEP and constant Young's modulus 100 GPa. On the right side: elastic thickness distribution calculated with the ASEP and Young's modulus variation shows almost high elastic thickness values variation in the middle part of study area (at longitude 40º E).*

The western margin bordering the continent-ocean transition is characterized by low rigidity-elastic thickness values, which indicate a weak crust. This result is in a very good agreement with the fact that this margin represents a shear margin, that was developed between north Greenland and the western margin of the Barents Shelf, forming a relay zone within the Arctic (Johansen et al., 1992).

The transition between the Western and Eastern Barents Sea in the central part of the study area is characterized by very high elastic thickness values < 60km.

It was already shown that the locations and directions of faults and tectonically units correlate with the areas of a rapid change of the elastic thickness or flexural rigidity values (Wienecke, 2006; Wienecke et al., 2007). For this reason it is proposed that the area of a rapid change from these high values to lower values should correlate with the presence of a suture zone or an old plate boundary (violet dotted line).

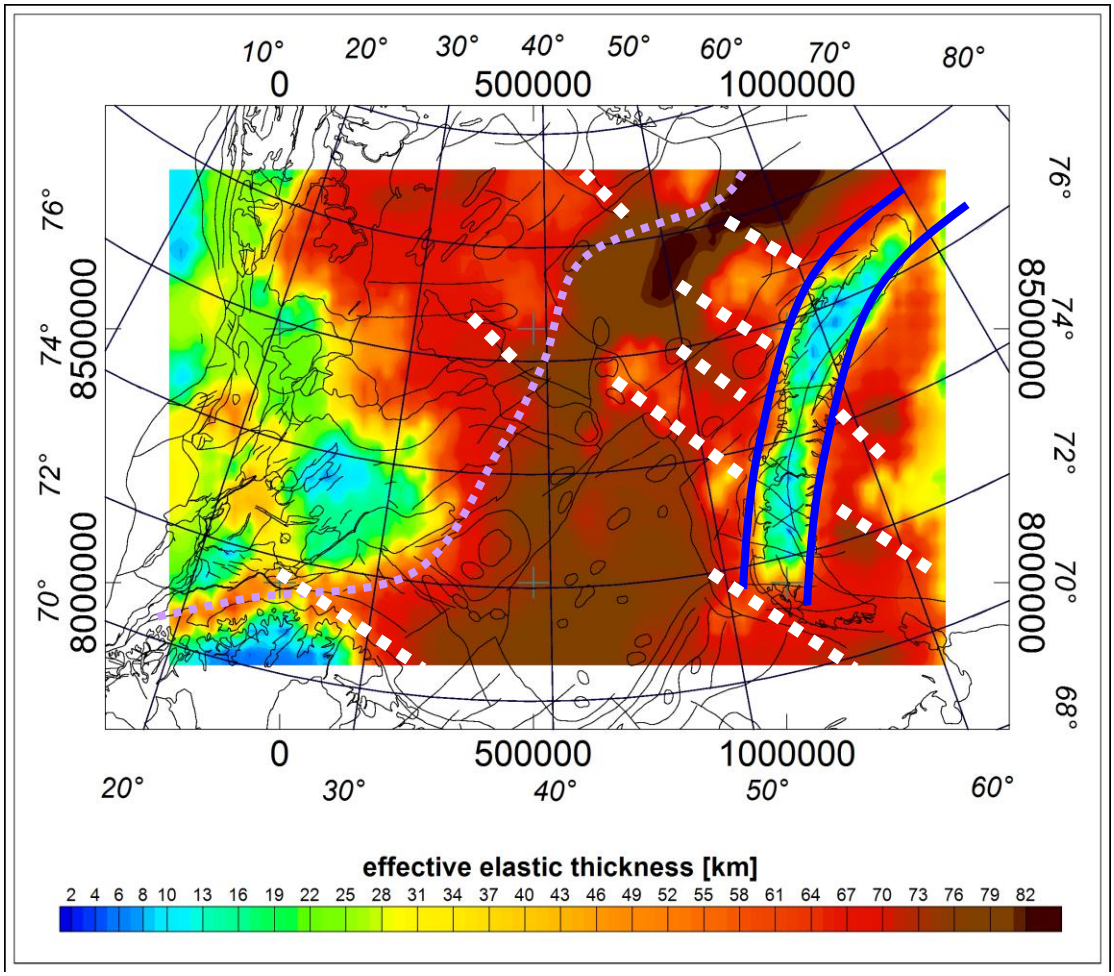

Figure 39 *Elastic thickness / flexural rigidity distribution taking a Young's modulus variation into account. Preliminary interpretation: Uralian trend marked by blue colored line, Timanide trend marked by white dotted line and the Caledonian suture zone marked by violet dotted line.*

The eastern Barents Sea is characterized by higher effective elastic thickness values (Figure 39), which indicate a rigid crust. This is in agreement with the fact, that this area was affected by a younger collision phase between the Laurentsian continent and Western Siberia. The eastern side of the Caledonides was flanked by the Timanides, that is recognized from the Finmark Platform up to the Timan-Pechora and Novaya-Zemlya region (Gee, 2005). Within the area of higher effective Te values (> 65 km) are trends of lower values (55 km) obtained. These lineaments strike in NE-SW direction (white dotted lines) and can be interpreted as Timanide trends. These structures are interrupted by the proposed Caledonian trend (violet dotted line). The foreland sedimentary basins immediately to the west of Novaya Zemlya show effective Te values of about 35 to 40 km. They formed in the foredeep zone to the Uralian thrustbelt.

The Ural Orogen mostly affects the eastern part of the Barents Sea. The Ural mountain chain and its proposed northern extension, Novaya Zemlya, likely mark the suture zone of this thrustbelt (Gee and Pearse, 2006). It is supposed that the structures (marked with blue line) are related to a Uralian trend (pers. comm. L. Gernigon 2007).

In summary, the study area in the Barents Sea is characterized in the western part by relatively small elastic thickness values and rift type sedimentary basins. On the other hand the eastern part is characterized by high Te values and shows large-scale intra cratonic basins. However, these preliminary interpretations should be discussed in future. Further investigations have to be carried out, especially with regard to the reliability and resolution of the used database.

4 CONCLUSION

3D density forward modelling and isostatic considerations clearly give evidence for a regional different density distribution in the lithospheric mantle below the Barents Sea Region. The result of a inhomogenous upper mantle correlates with the results of seismic tomography (Faleide et al. 2006) that distinguish a high-velocity structure in the lithospheric mantle bending parallel to Novaya Zemlya and deepening below it.

The difference of a planar and spherical 3D density model in terms of calculation of the gravity effect was investigated. The effect of the Earth's curvature is $15 \cdot 10^{-5} m/s^2$.
The effect is significant, nevertheless it is not enough to minimize the regional difference between the calculated and observed gravity.

The calculation of the elastic thickness shows, that it is important to take the Young's modulus variation into account. A formula was derived in order to calculate the effective Youngs modulus for a vertical and horizontal variation by using the information about the P-wave velocities.

All the results (mantle density, effective Youngs modulus and equivalent elastic thickness distribution) show clear evidence for large differences in physical properties between the Eastern and Western Barents Sea. The result based on the input data indicates that two different crustal plates exist with a transition zone between them, which is characterized by high effective elastic thickness values and a rapid change from high to low values. This is a common observation for the location of a suture zone.

However, these results have to be tested for feasibility in plate tectonic scenarious. The interpretation of trends in the effective elastic thickness distribution is preliminary. Further investigation concerning the correlation with geological observation and results from plate reconstruction modelling has to be carried out.

5 OUTLOOK

The 3D density model was further modeled against a reference model and the mantle densities were estimated by gravity inversion. A precise modeling and adjustment of the calculated gravity to the observed gravity requires a better resolution of the 3D model. The resolution of the model has to be improved by modeling along seismic lines. This is a task for future work and will be carried out in the PETROBAR project.

ACKNOWLEDGEMENTS

The work especially benefit from the cooperation with Carla Braitenberg from the University Trieste, Italy. She is inventor of the software LithoFLEX. Hans Morten Bjørnseth and Christine Fichler from Statoil initiated and supported the project BASIC. The continental shelf geophysics group and the geodynamic group from the NGU are thanked for support and discussion, especially Cécile Barrère, Odleiv Olesen and Trond Torsvik. For helpful discussions and the pre-publication release of information on the BARENTS50 model, Oliver Ritzmann, Jan Inge Faleide and Asbjørn Breivik are thanked.

REFERENCES

Ashby, M. and Jones, D.R.H., 2005. Engineering Materials, 1. Butterworth-Heinemann, 448 s.

Braitenberg, C., Wienecke, S., Ebbing, J., Born, W. and Redfield, T., 2007. Joint gravity and isostatic analysis for basement studies - a novel tool. EGM 2007 International Workshop, "Innovation in EM, Grav and Mag Methods: A new perspective for exploration." Capri, Italy.

Braitenberg, C., Wienecke, S. and Wang, Y., 2006. Basement structures from Satellite Derived Gravity Field: the South China Sea Ridge. Journal of Geophysical Research-Solid Earth, 111, B05407.

Breivik, A.J. et al., 2005. Caledonide development offshore-onshore Svalbard based on ocean bottom seismometer, conventional seismic, and potential field data. Tectonophysics, 401(1-2), 79-117.

Calcagnile, G., 1982. The lithosphere-asthenosphere system in Fennoscandia. Tectonophysics, 90, 19-35.

Christensen, N.I., 1978. Ophiolites, seismic velocities and oceanic crustal structure. Tectonophysics, 47, 131-157.

Crowley, Q.G., Floyd, P.A., Winchester, J.A., Franke, W. and Holland, J.G., 2000. Early Palaeozoic rift-related magmatism in Variscan Europe: fragmentation of the Armorican Terrane Assemblage. Terra Nova, 12 (4), 171-180.

Dziewonski, A.M. and Anderson, D.L., 1981. Preliminary reference earth model. Phys. Earth. Plan. Int., 25, 297-356.

Ebbing, J., Braitenberg, C. and Wienecke, S., 2007. Insights into the lithospheric structure and the tectonic settings of the Barents Sea region by isostatic considerations. Geophysical Journal International, 171 (3), 1390-1403.

Faleide, J.I., Myhre, A.M. and Eldholm, O., 1988. Early Tertiary volcanism at the western Barents Sea margin. In A.C. Morton & L.M. Parson (eds.) Early Tertiary Volcanism and the Opening of the NE Atlantic. Geological Society of London Special Publications, 39, 135-146.

Faleide, J.I., Ritzmann, O., Weidle, C. and Levshin, A., 2006. Geodynamical aspects of a new 3D geophysical model of the greater Barents Sea region- Linking sedimentary basins to the upper mantle structure. Geophysical Research Abstracts, 8, 08640.

Fichler, C., Rundhovde, E., Johansen, S. and Sæther, B.M., 1997. Barents Sea tectonic structures visualized by ERS1 satellite gravity data with indications of an offshore Baikalian trend. . First Break, 15, 355-363.

Föll, H., 2007. Manuscript to lectures of engineering materials, Modul 7.4.1., CAU Kiel, web resource http://www.tf.uni-kiel.de/matwis/amat/mw1_ge/.

Gee, D. and Pearse, V., 2006. The Neoproterozoic Timanide Orogen of eastern Baltica. Geological Society of London Memoirs, 30, 1-3.

Gee, D.G., 2004. The Barentsian Caledonides: Death of the High Arctic Barents Craton. In: M. Smelror and T. Brugge (Editors), Arctic Geology, Hydrocarbon Resources and Environmental challenges. . Geological Society of Norway, 48-49.

Gee, D.G., 2005. Scandinavian Caledonides (with Greenland) Elsevier, Uppsala.

Gramberg, I.S. et al., 2001. Eurasian Artic Margin: Earth Science Problems and Research Challenges. Polarforschung, 69, 3-15.

Gudlaugsson, S.T., Faleide, J.I., Fanavoll, S. and Johansen, B., 1987. Deep Seismic-Reflection Profiles across the Western Barents Sea. Geophysical Journal of the Royal Astronomical Society, 89(1), 273-278.

Gudlaugsson, S.T., Faleide, J.I., Johansen, S.E. and Breivik, A.J., 1998. Late Palaeozoic structural development of the South-western Barents Sea. Marine and Petroleum Geology, 15(1), 73-102.

International Association of Geodesy, 2002. Arctic Gravity Project- Data Set Information of National Geospatial-Intelligence Agency (NGA), web resource http://earth-info.nga.mil/GandG/wgs84/agp/readme.html..

Johansen, S.E., Ostisty, B.K., Birkeland, Ø., Federovski, Y.F., Martirosjan, V.N., Christensen, O.B., Cheredeev, S.I., Ignatenko, E.A. and Margulis, L.S., 1992. Hydrocarbon potential in the Barents Sea region: play distribution and potential. . In: Vorren, T.O., Bergsager, E., Dahl-Stamnes, Ø.A., Holter, E., Johansen, B., Lie, E. and Lund, T.B. (Editors), Arctic Geology and Petroleum Potential. Norwegian Petroleum Society Special Publication. Elsevier, Amsterdam, 273-320.

McKenzie, D., 1978. Some remarks on the development of sedimentary basins. Earth and Planetary Science Letters, 40, 25-32.

Pickering, K.T. and Smith, A.G., 1998. The Caledonides. In: B.A. Van der Pluijm and S. Marshak (Editors), Earth Structure: An Introduction to Structural Geology and Tectonics. W.W. Norton and Company, New York, 593-606.

Popowski, T., Connard, G. and French, R., 2006. GMSYS-3D: 3D Gravity and Magnetic Modeling for OasisMontaj - User Guide. Northwest Geophysical Associates, Corvallis, Oregon.

Ritzmann, O., Maercklin, N., Faleide, J.I., Bungum, H., Mooney, W.D. and Detweiler, S.T., 2006. A three-dimensional geophysical model of the crust in the Barents Sea region: model construction and basement characterization. Geophysical Journal International, 170(1), 417-435.

Skilbrei, J.R., 1991. Interpretation of Depth to the Magnetic Basement in the Northern Barents Sea (South of Svalbard). Tectonophysics, 200(1-3), 127-141.

Skilbrei, J.R., 1993. An evaluation of magnetic basement depth determinations from the southwestern Barents Sea. (Chapter eight). PHD Thesis, Norges tekniske høgskole, Trondheim, Norway.

Torsvik, T.H. and Andersen, T.B., 2002. The Taimyr fold belt, Arctic Siberia: timing of prefold remagnetisation and regional tectonics. Tectonophysics, 352, 335-348.

Tsikalas, F., 1992. A study of seismic velocity, density and porosity in Barents Sea wells (N. Norway). Master Thesis, University of Oslo - UIO, Oslo, Norway.

Weisstein, E.W., 1999. Sphere. From MathWorld, web resource: http://mathworld.wolfram.com/.

Wienecke, S., 2006. A new analytical solution for the calculation of flexural rigidity: significance and applications. PhD Thesis, Free University Berlin, Germany, web resource: http://www.diss.fu-berlin.de/2006/42/indexe.html.

Wienecke, S., Braitenberg, C., Ebbing, J. and Kukowski, N., 2006. Reinterpretation of the effective elastic thickness in terms of Young's modulus variation applying the analytical solution for an elastic plate (ASEP) to the Barents Sea. In: T. Watts et al. (Editor), poster session: Tectonophysics (T34), AGU Fall Meeting, San Francisco.

Wienecke, S., Braitenberg, C. and Götze, H.-J., 2007. A new analytical solution estimating the flexural rigidity in the Central Andes. Geophysical Journal International,169 (3), 789-794.

Wienecke, S., Gernigon, L. and Kukowski, N., 2008. Recalculation of the elastic thickness in terms of Young's modulus variation applying the analytical solution for an elastic plate (ASEP) to the greater Barents Sea region. Geophysical Journal

International, in preparation.

FIGURE CAPTIONS

NGU
Norges geologiske undersøkelse
Geological Survey of Norway

Norges geologiske undersøkelse
Postboks 6315, Sluppen
7491 Trondheim, Norge

Besøksadresse
Leiv Eirikssons vei 39, 7040 Trondheim

Telefon 73 90 40 00
Telefax 73 92 16 20
E-post ngu@ngu.no
Nettside www.ngu.no

Geological Survey of Norway
PO Box 6315, Sluppen
7491 Trondheim, Norway

Visitor address
Leiv Eirikssons vei 39, 7040 Trondheim

Tel (+ 47) 73 90 40 00
Fax (+ 47) 73 92 16 20
E-mail ngu@ngu.no
Web www.ngu.no/en-gb/